

Application of an Integrated Omics Approach for Identifying Host Proteins That Interact With *Odontoglossum ringspot virus* Capsid Protein

Pin-Chun Lin,^{1,2} Wen-Chi Hu,¹ Shu-Chuan Lee,¹ Ying-Lan Chen,^{4,5} Chi-Ying Lee,⁴ Yet-Ran Chen,⁴ Li-Yu Daisy Liu,⁶ Po-Yen Chen,¹ Shih-Shun Lin,^{2,3,4} and Ya-Chun Chang¹

¹Department of Plant Pathology and Microbiology, National Taiwan University, 1, Sec. 4, Roosevelt Rd., Taipei, Taiwan;

²Institute of Biotechnology, National Taiwan University, 81, Chang-Xing St., Taipei, Taiwan; ³Genome and Systems Biology Degree Program, National Taiwan University, 1, Sec. 4, Roosevelt Rd., Taipei, Taiwan; ⁴Agricultural Biotechnology Research Center, Academia Sinica, 128, Academia Rd, Sec. 2, Taipei, Taiwan; ⁵Institute of Plant Biology and Department of Life Science, National Taiwan University, 1, Sec. 4, Roosevelt Rd., Taipei, Taiwan; ⁶Department of Agronomy, National Taiwan University, 1, Sec. 4, Roosevelt Rd., Taipei, Taiwan

Submitted 26 August 2014. Accepted 19 January 2015.

The glutamic acid at position 100 (E¹⁰⁰) in the capsid protein (CP) of *Odontoglossum ringspot virus* (ORSV) plays an important role in long-distance viral movement in *Nicotiana benthamiana*. The ORSV^{E100A} mutant, which has a glutamic acid to alanine substitution, shows a loss of systemic infectivity in *N. benthamiana*. Transmission electron microscopy and size-exclusion chromatography assays showed that E¹⁰⁰ is essential for CP-CP interaction and viral particle assembly. To identify the ORSV triggering or response genes and CP-interacting proteins (CP-IP), an integrated omics approach based on next-generation sequencing and proteomics profiling was used in this study. The whole-transcriptomes of healthy and ORSV-infected leaves of *N. benthamiana* were analyzed, and the gene information was used to create a *N. benthamiana* protein database that was used for protein identification following mass spectrometry analysis. The integrated omics approach identified several putative host proteins that interact with ORSV CP^{WT} and were categorized as photosystem subunits, defense-associated proteins, and cell division components. The expression pattern and CP interaction of these CP-IP were examined by semiquantitative reverse transcription polymerase chain reaction and an *in vitro* binding assay, respectively, to verify the *in silico* data. Among these proteins, a proteinase inhibitor of *N. benthamiana* (NbPI2) was highly associated with CP^{E100A} as compared with CP^{WT}, and NbPI1 and NbPI2 were highly induced in ORSV-infected plants. NbPI1- and NbPI2-silenced plants (via a *Tobacco rattle virus*-induced gene-silencing system) did not exhibit a difference in ORSV infection. Thus,

whether NbPI1 and NbPI2 play a role in plant immunity requires further investigation. In summary, the integrated omics approach provides massive and valuable information to identify the ORSV CP-IP and these CP-IP will help us to understand the movement of this virus and plant-virus interaction.

Odontoglossum ringspot virus (ORSV) belongs to the genus *Tobamovirus*, which was originally isolated from the orchid *Odontoglossum grande* and threatens the orchid industry worldwide (Adams et al. 2009; Hong et al. 2011; Khentry et al. 2006; Rabindran et al. 2005; Wong et al. 1994). ORSV has been reported that can infect Chenopodiaceae and Solanaceae families in nature, including *Nicotiana benthamiana*, with systemic infection (Hilf and Dawson 1993). The laboratory-created mutant ORSV^{E100G} has a Glu100Gly mutation on the ORSV capsid protein (CP) that was generated by fragment swapping, and this mutant virus lost its systemic movement ability in *N. benthamiana*, resulting in nonsystemic infection (Lee 2008). Many reports have indicated that *Tobacco mosaic virus* (TMV) mutants with a CP gene deletion also exhibited systemic movement deficiencies (Dawson et al. 1988; Holt and Beachy 1991; Takamatsu et al. 1987). Yu and Wong (1998) reported that the systemic spread of CP-deleted ORSV was greatly reduced. These findings suggested that the CP of tobamoviruses play an important role in systemic infection.

A tobacco protein, *Tomato mosaic virus* (ToMV) CP-IP-L (interacting protein-L), has been shown to assist in viral systemic movement (Li et al. 2005; Zhang et al. 2008). Pectin methylesterase (PME) interacts with the TMV movement protein (MP), which is responsible for virus cell-to-cell movement (Chen et al. 2000). The virus loses its systemic infection ability when the MP gene was mutated or wild-type TMV was infected on the PME knock-down tobacco plants (Chen and Citovsky 2003; Chen et al. 2000). Furthermore, a transgenic tobacco plant expressing the cadmium ion-induced glycine-rich protein (*cdiGRP*) gene, which is a low cadmium-inducing cell-wall component, was shown to block *Turnip vein-clearing virus* systemic movement (Ueki and Citovsky 2002). These results indicate that host components are involved in viral systemic movement. However, the limited number of identified CP-IP does not allow the mechanism of systemic movement to be studied. Identification of additional CP-IP candidates is required for

The raw transcriptome reads reported in this paper are available in the NCBI Short Read Archive under accession numbers SRR1552497 (healthy *N. benthamiana*) and SRR1552498 (ORSV-infected *N. benthamiana*). The transcriptome contig sequences of *N. benthamiana* are available in the ContigViews database.

Corresponding authors: S.-S. Lin; Telephone: +886-2-3366-6023; Fax: +886-2-3366-6001; E-mail: linss01@ntu.edu.tw; and Y.-C. Chang; Telephone: +886-2-3366-5209; Fax: +886-2-2362-0271; E-mail: ycchang@ntu.edu.tw

*The e-Xtra logo stands for “electronic extra” and indicates that two supplementary figures and four supplementary tables are published online.

characterizing the host-pathogen interaction network via a high-throughput systems biology approach.

The development of next-generation sequencing (NGS) has enabled whole-transcriptomic analyses of nonmodel organisms (Liu et al. 2014; Su et al. 2011; Van Moerkercke et al. 2013). Approximately 20,000 to 40,000 genes can be identified through NGS analysis and high-throughput reads of these transcriptomes can be converted to fragments per kilobase of transcript per million mapped reads (FPKM) or DESeq to represent differential expression (Howe et al. 2011). In plant pathology, the NGS technique has been applied to study phytoplasma-mediated leafy flower symptom development in *Catharanthus roseus* (Liu et al. 2014). The relational network among different genes was used to formulate a hypothesis to explain the mechanism of leafy flower symptoms (Liu et al. 2014), indicating the power of NGS in the study of plant-pathogen interactions. Whole-transcriptome sequencing is independent of genome sequence and provides precise amino acid sequences for mass spectrum predictions in proteomics studies.

Guarnieri et al. (2011) demonstrated that the de novo transcriptome of microalgae can be used for proteomic analyses, and several genes that are involved in the fatty acid and triacylglycerol biosynthetic machinery were identified. Furthermore, Van Moerkercke et al. (2013) combined transcriptome profiles and metabolic networks from omics data to reconstruct a metabolic pathway and discover missing enzymes for engineering metabolic study. Therefore, we define the “integrated omics approach” as a novel discovering strategy combining multiple high-throughput profiles to find new research directions.

To study the molecular mechanisms underlying the *N. benthamiana*-ORSV interactions and viral systemic movement, we created a new ORSV CP mutant virus, ORSV^{E100A} that contains a restriction fragment length polymorphism (RFLP) marker. Observations with transmission electron microscopy, size-exclusion chromatography, and an in vitro CP-CP interaction assay showed that CP^{E100A} leads to defective viral

particle assembly. In addition, an integrated omics approach that combined proteomics and transcriptomics assays were used to identify the specific CP^{WT}-IP from healthy and ORSV-infected *N. benthamiana* plants. Furthermore, several experimental approaches, including semiquantitative reverse transcription polymerase chain reaction (RT-PCR), an in vitro binding assay, and virus-induced gene silencing (VIGS), were used to verify the differential expression, physical interaction, and gene function of these CP^{WT}-IP. Furthermore, one of the identified CP-IP, *NbPI2*, was shown to be upregulated in ORSV-infected plants and strongly interacted with CP^{E100A}. The possible function of *NbPI2* in ORSV infection was proposed in this study.

RESULTS

The conserved glutamic acid at position 100 (E¹⁰⁰) residue in the CP of tobamoviruses.

Our previous results showed that E¹⁰⁰ of the ORSV CP plays an important role in viral systemic movement in *N. benthamiana* (Lee 2008). The alignment of the CP sequences of tobamoviruses indicated that 10 out of 13 species have an E¹⁰⁰ residue, *Tobacco mild green mosaic virus* and *Obuda pepper virus* have an aspartic acid residue (D¹⁰⁰), and only *Cucumber green mottle mosaic virus* has a valine residue (V¹⁰⁰) (Fig. 1A). Because glutamic acid and aspartic acid are acidic amino acids with carboxylate groups as side chains and similar biochemical properties, this conserved E¹⁰⁰ in the CP may play an important role in virus infection. Based on the predicted three-dimensional structure of the CP protein, E¹⁰⁰ is located on the loop region, which is oriented on the inner surface of the CP subunit that may respond to viral particle assembly (Fig. 1B). To examine the importance of E¹⁰⁰, site-directed mutagenesis was performed on the pORSV^{WT} infectious clone (Lee 2008) to substitute the E¹⁰⁰ residue of CP with an alanine residue to generate pORSV^{E100A} (Fig. 1C). A restriction enzyme site, *MscI*, was incorporated at the mutation site to distinguish ORSV^{E100A} from ORSV^{WT}, using PCR-RFLP.

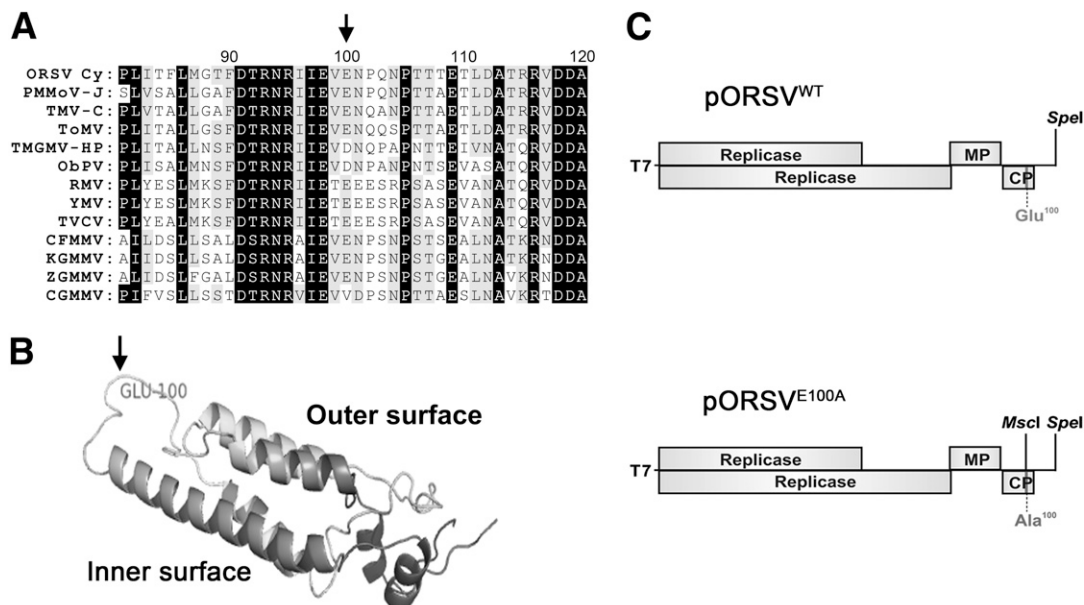


Fig. 1. The conserved amino acid (E¹⁰⁰) in the capsid protein (CP) of *Odontoglossum ringspot virus* (ORSV). **A**, Amino acid sequence alignment of ORSV CP with other tobamoviruses. The arrow indicates the conserved glutamic acid (E) residue at the 100th position. **B**, Predicted three-dimensional structure of ORSV CP. Four alpha helix structures and two loops are shown. The indicated E¹⁰⁰ residue is located on the loop of the inner surface of the virus particle. **C**, Schematic representations of the genomes of the T7 promoter-driven wild-type (ORSV^{WT}) and mutant (ORSV^{E100A}) ORSV full-length cDNA clones pORSV^{WT} and pORSV^{E100A}, respectively. The 126-kDa replicase, 183-kDa replicase of the read-through form, 31-kDa movement protein (MP), and 18-kDa CP are shown. The only variability between the two clones is the change from E¹⁰⁰ to A¹⁰⁰ on the CP. The *MscI* restriction enzyme site was created by polymerase chain reaction-based mutagenesis, and the *SpeI* restriction enzyme site was used to linearize the DNA template for in vitro transcription.

The infectivity assay of ORSV in *N. benthamiana* and *Chenopodium quinoa*.

The in vitro transcripts of pORSV^{WT} and pORSV^{E100A} were transfected into protoplasts of *N. benthamiana*. The results of the Northern blot analysis showed that ORSV^{WT} and ORSV^{E100A} replicated equally in single cells (Supplementary Fig. 1). However, ORSV^{E100A} did not cause any symptoms on the systemic leaves of *N. benthamiana*, while inoculation with ORSV^{WT} caused leaf curl symptoms in systemic leaves at 10 days postinoculation (dpi) (Fig. 2A). The RFLP results showed that the *MscI*-treated RT-PCR products of ORSV^{E100A} were digested into 300- and 185-bp fragments, whereas those from the ORSV^{WT} fragments remained uncut (485 bp) (Fig. 2B). The results of the Western blot analysis also confirmed that ORSV^{E100A} was only detected in inoculated leaves but not in systemic leaves at 10 dpi, whereas ORSV^{WT} could be detected in both types of leaves (Fig. 2C). Even at 30 dpi, ORSV^{E100A} still was not detected in the systemic leaves (data not shown). The difference in the protein mobility between CP^{WT} and CP^{E100A} was detected using Western blot analysis (Fig. 2C). *C. quinoa* was used to examine the cell-to-cell movements of both viruses. No differences in lesion formation, including number and size, were observed between the two viruses (Fig. 3A). These results demonstrated that the E¹⁰⁰A mutation in the CP greatly affected the systemic movement of ORSV in *N. benthamiana*. In addition, two molecular markers, including RFLP and CP protein mobility, provided convenient means for tracing ORSV^{WT} and ORSV^{E100A}.

CP^{E100A} altered the CP-CP interaction and viral particle assembly.

We first examined whether the E¹⁰⁰A mutation affects viral particle assembly through morphological observations, using immunosorbent electron microscopy (ISEM) (Fig. 3A). The ISEM data showed that ORSV^{WT} viral particles were approximately 300 nm in length (Fig. 3A and B). The particle lengths of ORSV^{E100A}, however, were diverse and ranged from

approximately 130 to 460 nm (Fig. 3A and B), thus demonstrating aberrant particle assembly. Next, we performed a size-exclusion chromatography analysis to further analyze viral particles from infected plants. The results showed that CP of ORSV^{WT} was primarily detected in high molecular-weight fractions, suggesting that most of the CPs formed viral particles in infected plants (Fig. 4A, upper panel). In contrast, the CP of ORSV^{E100A} was primarily detected in low molecular-weight fractions, and less CP^{E100A} was detected in the high molecular-weight fractions, suggesting that CP^{E100A} is less efficient at particle assembly (Fig. 4A, lower panel).

Virus particle assembly is correlated with the CP-CP interaction. Therefore, CP self-interaction was evaluated using an in vitro pull-down assay. CP^{WT}-His or CP^{E100A}-His was used as bait to test the CP-CP binding ability with glutathione *S*-transferase (GST)-CP^{WT} and GST-CP^{E100A}. The data showed that GST-CP^{WT} + CP^{WT}-His has the strongest interaction in different concentrations of Triton X-100 relative to GST-CP^{WT} + CP^{E100A}-His, GST-CP^{E100A} + CP^{WT}-His, and GST-CP^{E100A} + CP^{E100A}-His (Fig. 4B). This result demonstrated that the substitution of residue E¹⁰⁰ with A¹⁰⁰ altered the binding affinity of the CP subunits. In summary, our data indicated that CP^{E100A} loses its ability to form viral particles of the correct size and, therefore, might result in the defective systemic movement of ORSV^{E100A} in *N. benthamiana*. In addition, the E¹⁰⁰A substitution on the ORSV CP might alter the interaction between the CP and host components, resulting in deficiencies of systemic movement or viral infection.

Integrated omics approach with an experimental validation for CP interaction study.

In addition to viral particle assembly, the CP-host component interaction also plays an important role in viral infection and defense response (Li et al. 2005; Karran and Sanfaçon 2014). In this study, an integrated omics approach that combines the whole-transcriptome and proteome was used to

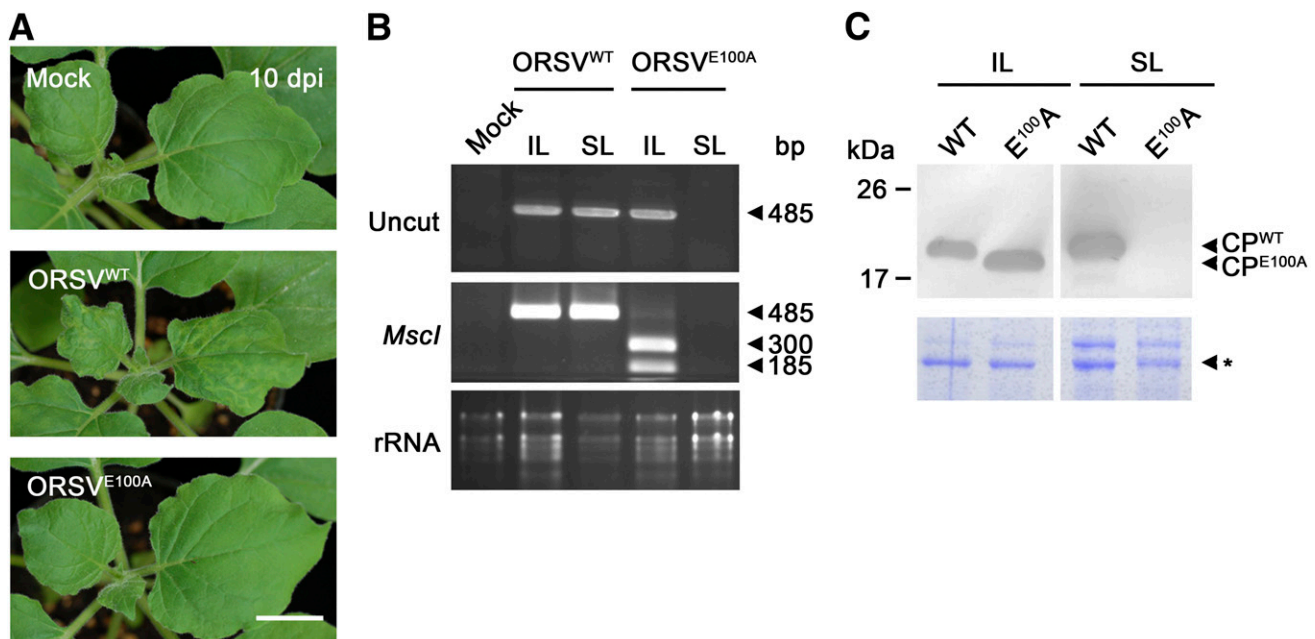


Fig. 2. The E¹⁰⁰ residue of the *Odontoglossum ringspot virus* (ORSV) capsid protein (CP) contributes to viral infectivity on *Nicotiana benthamiana*. **A**, Symptoms of mock- and ORSV-inoculated *N. benthamiana* plants. Photographs were taken at 10 days postinoculation (dpi). Bar = 1 cm. **B**, Reverse transcription-polymerase chain reaction (RT-PCR) and restriction fragment length polymorphism analysis of inoculated (IL) and systemic (SL) leaves from mock-, ORSV^{WT}-, and ORSV^{E100A}-infected plants at 10 dpi. The uncut (upper panel) and *MscI*-digested (middle panel) RT-PCR products of CP genes and rRNAs (lower panel) are shown. **C**, CP accumulation in IL and SL of mock-, ORSV^{WT}-, and ORSV^{E100A}-infected plants was analyzed by Western blot analysis with an anti-ORSV CP antibody at 10 dpi. Rubisco was used as the loading control (lower panel).

identify the CP-IP and their expression profiles (Fig. 5A and B). The transcriptomic sequence provides a precise mass spectrum for proteomic predictions by bioinformatics (Fig. 5C). Finally, these candidate CP-IP can be verified through experimental validation, including semiquantitative RT-PCR, in vitro binding assays, and VIGS (Fig. 5D).

Whole-transcriptome analysis and gene expression of *N. benthamiana*.

To obtain a comprehensive gene expression profile of *N. benthamiana*, healthy and ORSV^{WT}-infected plants were analyzed, based on their whole-transcriptome profiles, using NGS. We obtained 26,201,860 raw reads from healthy plants and 27,266,778 reads from ORSV^{WT}-infected plants (Fig. 5A). These reads were mixed for de novo assembly, and 84% of the reads were successfully assembled into 85,599 contigs. These contigs were analyzed using the basic local alignment search tool (BLAST) with an *Arabidopsis thaliana* coding sequence (CDS) database (TAIR 10) and an European Molecular Biology Laboratory (EMBL) CDS database for name-calling and open reading frame (ORF) annotation. The annotation results identified 5,436 complete contigs (6%) and 35,123 partial contigs (41%) (Figs. 5A and 6A). All of the contig sequence information and annotation results were integrated into ContigViews to develop a *N. benthamiana* transcriptome database.

The 5,436 complete contigs from *N. benthamiana* were compared for similarities with *Arabidopsis* CDS. The lengths of the matched CDS between *N. benthamiana* and *Arabidopsis* are highly correlated ($R = 0.993$), and the majority of the genes were identical in length to their homologs in *Arabidopsis* (Fig. 6B and C). The average amino acid similarity was approximately 50% (Fig. 6D). In addition, 12,135 of 40,559 genes showed more than 50% coverage in the reference sequence

(Supplementary Table 1). Of 12,135 genes, 30% showed two-fold differential expression during ORSV infection (Fig. 7A). The gene set enrichment analysis (GSEA) results indicated that many genes were involved in metabolic processes, stress response, and chloroplast development (Table 1). Therefore, these results suggested that ORSV infection triggers the host defense response and interferes with chloroplast development.

Next, 40,559 *N. benthamiana* genes (including complete and partial genes) were used to predict the protein mass database and were then integrated into MASCOT for further proteomics analysis (Figs. 5C and 6A).

Protein identification using the *N. benthamiana* transcriptome database.

The coimmunoprecipitation and liquid chromatography-tandem mass spectrometry (LC-MS/MS) approaches were employed to identify the ORSV CP-IP (Fig. 5B). The results showed that CP coimmunoprecipitated with possible CP-interacting host proteins from extracts of ORSV^{WT}- and ORSV^{E100A}-infected plants (Fig. 8A). Entire lanes of the three coimmunoprecipitation products (healthy, ORSV^{WT}, and ORSV^{E100A}) were analyzed by LC-MS/MS after in-gel digestion (Fig. 8A). The mass results were analyzed by MASCOT with the ContigViews *N. benthamiana* transcriptome database (Fig. 5B and C).

A total of 51 proteins correlated to the transcriptome contigs were identified from coimmunoprecipitation products of CP^{WT} and CP^{E100A} that were filtered to remove false positive proteins from the LC-MS/MS profile of healthy plants and were considered as the putative ORSV CP-IP (Tables 2 and 3). ORSV CP was among the proteins identified from both the CP^{WT}- and CP^{E100A}-infected samples, indicating that the coimmunoprecipitation and LC-MS/MS processes were successful (Fig. 8A). Most of the IP identified from the CP^{WT} and CP^{E100A} fractions were photosystem subunits,

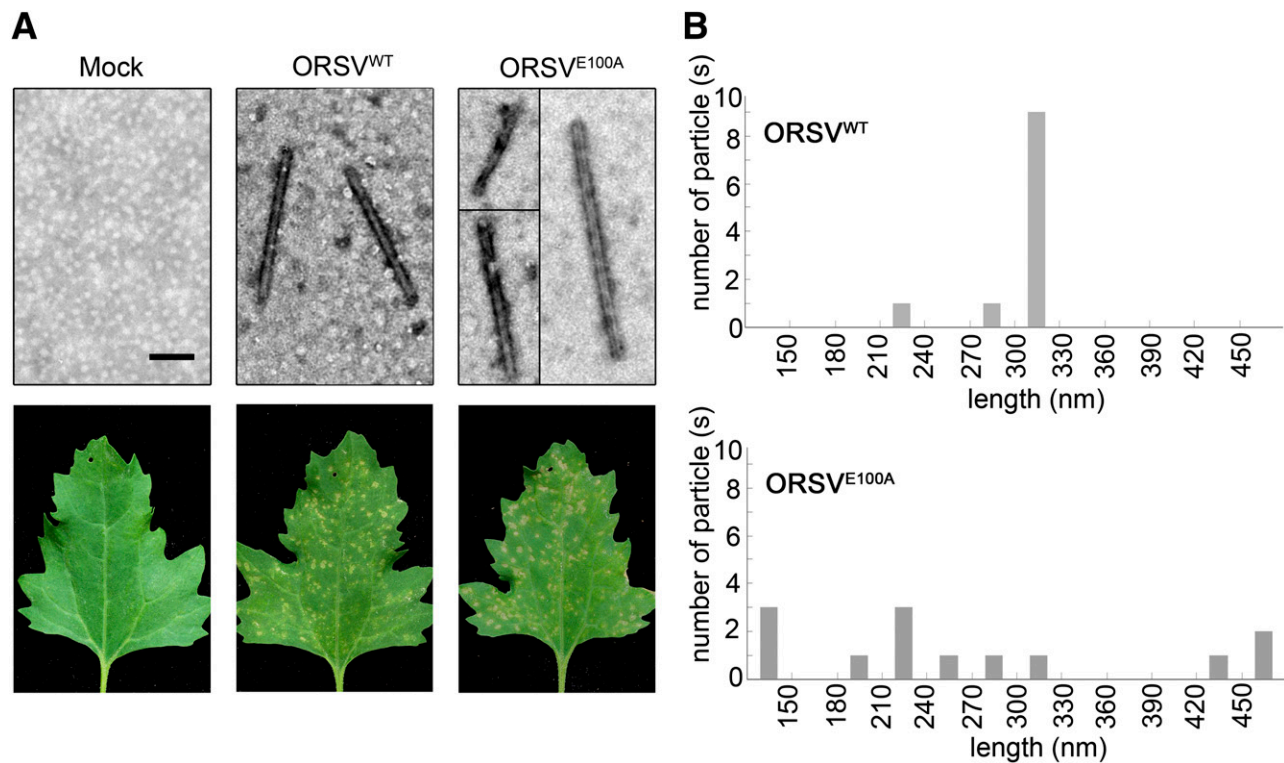


Fig. 3. Observation of *Odontoglossum ringspot virus* wild type (ORSV^{WT}) and ORSV^{E100A} viral particles by immunosorbent electron microscopy (ISEM). **A**, Local lesion formation on mock- and ORSV-inoculated *Chenopodium quinoa* was observed at 4 days postinoculation. ISEM was performed with an anti-ORSV capsid protein antibody. Antibody-decorated viral particles of ORSV^{WT} and ORSV^{E100A} derived from inoculated *C. quinoa* are shown. Bar = 100 nm. **B**, The particle length distribution of ORSV^{WT} (upper) and ORSV^{E100A} (lower) virions.

suggesting that ORSV might affect the chloroplasts through CP-photosystem subunit interactions (Table 2).

CP^{WT}-IP.

In this study, we focused on the CP^{WT}-IP, in which the real viral infection can be reflected. Thirty CP^{WT}-IP genes with differential in silico expression between mock- and ORSV-infected plants were identified (Table 3). For *NbRCA* (NBOR457), whose ortholog in *Arabidopsis* is a ribulose-1,5-bisphosphate carboxylase (Rubisco) activase, expression

was down-regulated in ORSV-infected plants (Fig. 7Bi and D; Table 3), whereas the expression of *NbHLL1* (NBOR18678) was up-regulated (Fig. 7Bii and D; Table 3). Both orthologs in *Arabidopsis* have also been reported to be involved in photosystems (Boex-Fontvieille et al. 2014; Portis 2003; Sureshkumar et al. 2009).

The orthologous genes of *NbGOX1* (NBOR1162) and *NbSHM1.1* (NBOR327) in *Arabidopsis* have been demonstrated to be involved in oxygen species metabolic pathways (Chern et al. 2013; Fahnenstich et al. 2008; Zhou et al. 2012). Both genes were down-regulated in ORSV-infected plants (Fig. 7Biii and iv and D;

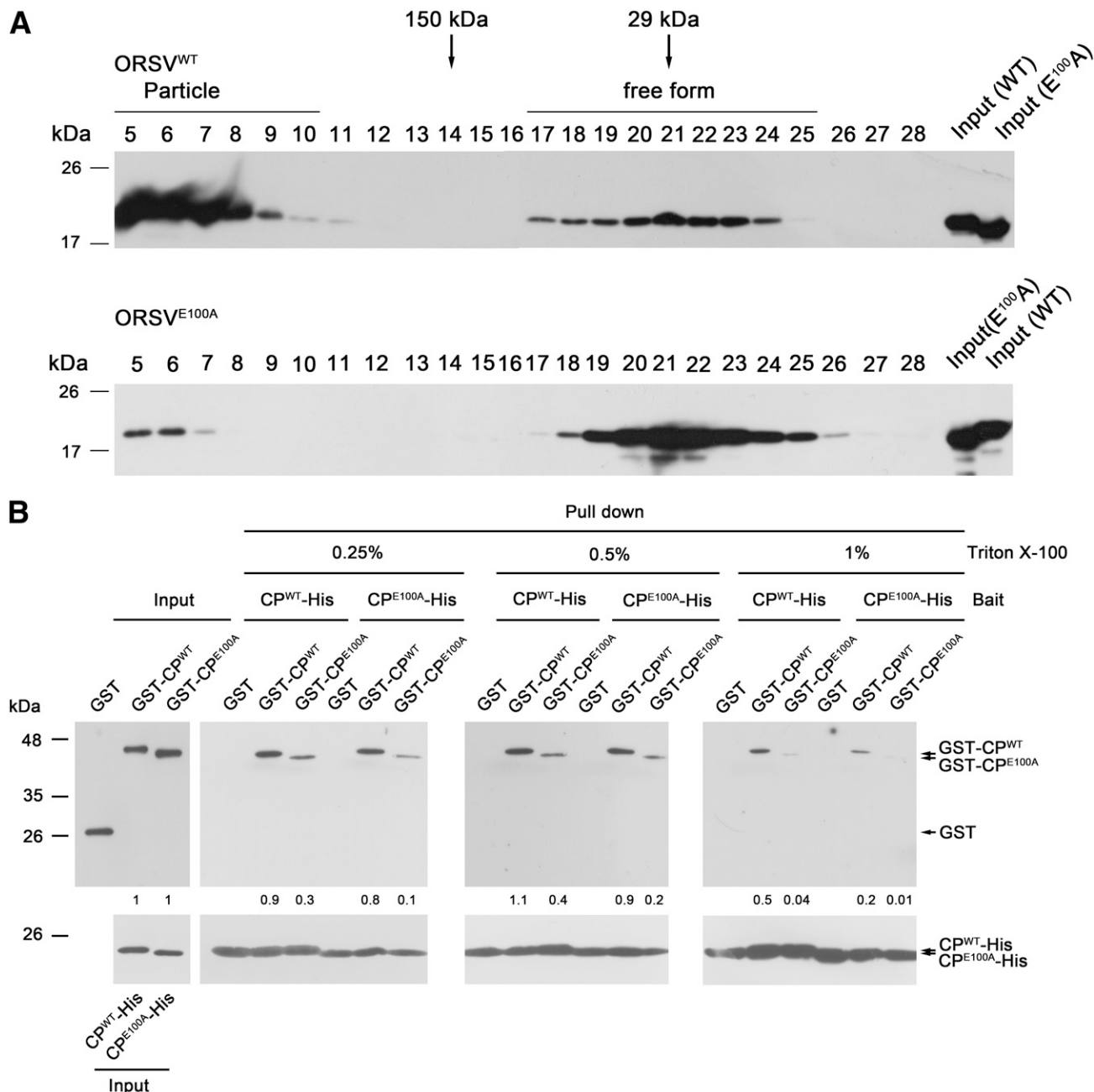


Fig. 4. Evaluation of viral particle assembly of *Odontoglossum ringspot virus* wild type (ORSV^{WT}) and ORSV^{E100A}. **A**, The capsid protein (CP) size distribution of ORSV^{WT} and ORSV^{E100A} in planta was analyzed using size-exclusion chromatography. The total protein extracts from ORSV^{WT}- and ORSV^{E100A}-infected *Nicotiana benthamiana* were size-fractionated on a gel filtration column. Fractions were analyzed by Western blot analysis with an anti-ORSV CP antibody. The numbers on the top of the panel indicate the fractions. The molecular sizes of the standards are indicated with arrows. **B**, In vitro CP-CP interaction assay of ORSV CP^{WT} and CP^{E100A}. Glutathione *S*-transferase (GST)-CP^{WT} or GST-CP^{E100A} and CP^{WT}-His or CP^{E100A}-His were assayed for in vitro CP-CP interaction using a pull-down assay. The bait (CP^{WT}-His or CP^{E100A}-His) was pulled down with Ni-NTA, and Western blot analysis was performed with an anti-GST polyclonal antibody. Different stringencies were created using various concentrations of Triton X-100 (0.25%, 0.5%, or 1%). The inputs (CP^{WT}-His, CP^{E100A}-His, GST, GST-CP^{WT}, and GST-CP^{E100A}) used in this study were verified by Western blot analysis with anti-His or anti-GST antibodies. The numbers indicate the relative fold change of pulled-down CP to the CP^{WT} or CP^{E100A} of inputs.

Table 3). In contrast, *NbNPC2* (NBOR6197), whose orthologs in *Arabidopsis* have been shown to be involved in the biotic stress response (Slaughter et al. 2012; Pokotylo et al. 2013), was up-regulated in ORSV-infected plants (Fig. 7Bv and D; Table 3). Moreover, *NbPIPI;4* (NBOR145), which is a member of the plasma membrane-intrinsic protein (PIP) family in *Arabidopsis* and involved in the response to chilling stress (Lee et al. 2012), was down-regulated in ORSV-infected plants (Fig. 7Bvi and D; Table 3).

In addition to the in silico expression of *CP^{WT}-IP*, in vivo RNA transcript expressions between mock and ORSV-infected plants were also confirmed by semiquantitative RT-PCR (Fig. 7D). *NbRCA*, *NbSHM1.1*, and *NbPIPI;4* were down-regulated

in ORSV-infected plants, whereas *NbNPC2* and *NbIIL1* were up-regulated. These results are consistent with the in silico profiles (Fig. 7B and D). The *NbGOX1* gene was not detected by semiquantitative RT-PCR.

Moreover, the *CP^{WT}-IP* were evaluated for their interaction with *CP^{WT}*. The pEXP5-CT/TOPO TA expression system (Invitrogen) and the Expressway Cell-Free *E. coli* Expression system (Invitrogen) were used for cloning of *CP^{WT}-IP* genes and in vitro recombinant protein expression. The *NbGOX1*, *NbIIL1*, *NbNPC2*, and *NbRCA* genes (partial ORF; sequence refers to the amino acids 129 to 270 of AtRCA) were successfully cloned and expressed by in vitro transcription and translation (Fig. 9A). Except for NbRCA-His, the *CP^{WT}-IP* showed interaction

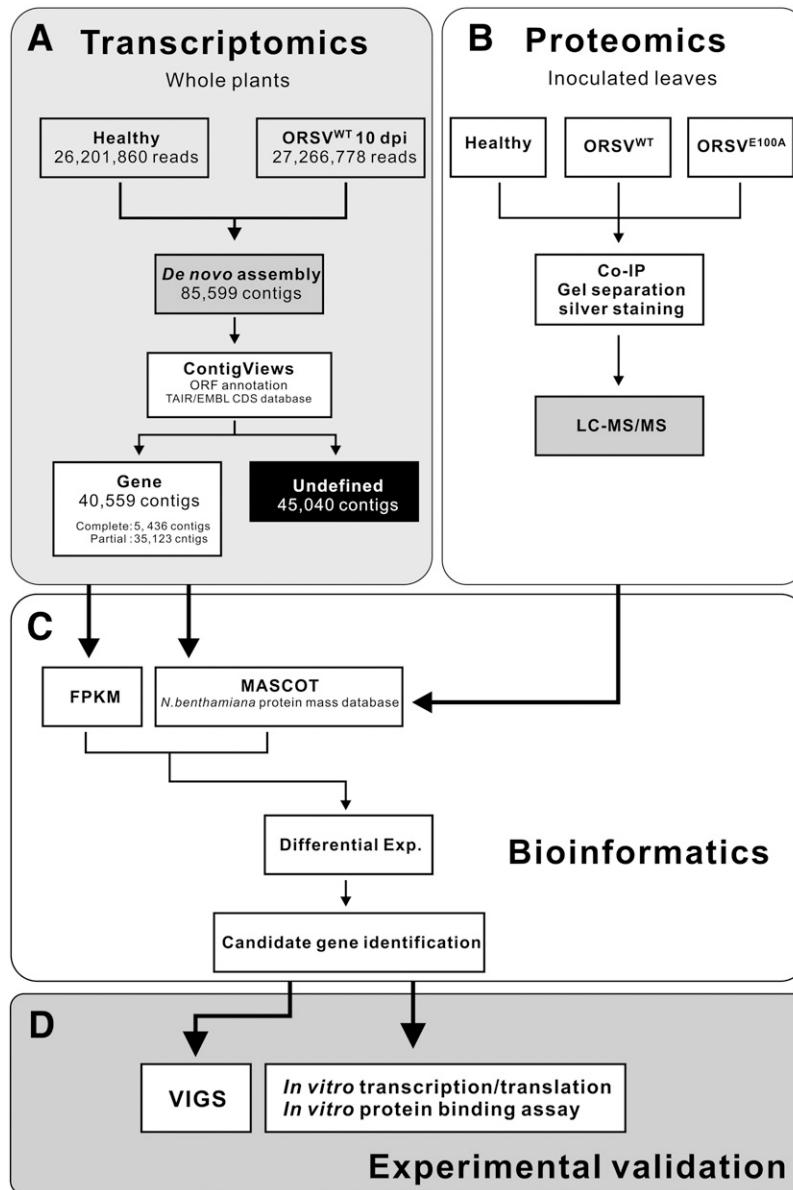


Fig. 5. Next-generation sequencing was used in the proteomics workflow and whole-transcriptome assays. **A**, Whole-transcriptome analysis pipeline. Healthy and *Odontoglossum ringspot virus* wild type (ORSV^{WT})-infected *Nicotiana benthamiana* plants at 10 day postinoculation were used for whole-transcriptome analysis by deep sequencing. The de novo assembly utilized mixed reads from two samples to generate *N. benthamiana* transcript contigs. Gene annotation and open reading frame finding was predicted using the ContigViews web server (Liu et al. 2014), and the amino acid sequences of these genes were used for protein mass prediction by MASCOT. **B**, Healthy, ORSV^{WT}-, and ORSV^{E100A}-infected *N. benthamiana* plants were used for proteomics analysis. The ORSV CP-interacting proteins (CP-IP) were isolated by immunoprecipitation with anti-ORSV CP antibodies from the total protein extracts. These co-immunoprecipitated proteins were separated by gel electrophoresis and were stained with the silver staining method. These elutes were analyzed using liquid chromatography-tandem mass spectrometry methods. **C**, The mass results were compared with the specific *N. benthamiana* mass database by MASCOT for the protein identification. The CP-IP were verified using the transcriptome database to identify the candidate genes involved in ORSV infection. **D**, The candidate CP-IP were evaluated for CP-binding ability and gene function through experimental approaches, including in vitro binding assay and virus-induced gene silencing (VIGS).

with CP^{WT} in vitro, confirming the coimmunoprecipitation proteomics results (Fig. 9B). In addition, variations of the prey signal intensities of the coimmunoprecipitation imply different binding affinities between CP^{WT} and CP^{WT}-IP (Fig. 9B). However, green fluorescent protein (GFP) + GST-CP^{WT} did not show an interaction and was used as a negative control (Fig. 9C). The lack of interacting signal between GST-CP^{WT} and NbRCA-His (Fig. 9B) may have been caused by the lower input of NbRCA-His (Fig. 9A) or the lack of a CP^{WT}-interacting domain in the partial NbRCA protein.

The other CP^{WT}-IP, such as *NbIBS1* (NBOR22975), *NbFIB4* (NBOR6354), *NbCNGC1* (NBOR12131), *NbAGT1* (NBOR316), *NbVCL1* (NBOR48019), and *NbSK21* (NBOR4906) are listed in Table 3. Their orthologous genes in *Arabidopsis* have been reported to be involved in biotic stress response, photosystems, ion channels, nutrition transport, vacuole development, and protein degradation (Hicks et al. 2004; Pokotylo et al. 2013; Singh et al. 2010; Slaughter et al. 2012; Wang et al. 2013; Zhang et al. 2013; Zhao et al. 2003). *NbFLN1* (NBOR16452) and *NbORC2* (NBOR45173) interact with CP^{WT} and their mRNA expressions were up-regulated in infected plants (Table 3). Moreover, a helicase-SANT-associated domain protein (NBOR6246) was identified and shown to interact with CP^{WT} (Table 3). These orthologous genes in *Arabidopsis* play a role in RNA expression, cell division, and nucleic acid binding, respectively (Bell and Dutta 2002; Gilkerson et al. 2012). The remaining 15 CP^{WT}- and 13 CP^{E100A}-IP that have not been characterized or have unclear functions are listed in Supplementary Table 2.

NbPI2 was enriched in CP^{E100A} coimmunoprecipitation products.

A 24-kDa protein was observed in the coimmunoprecipitation reaction of CP^{E100A}, whereas a weak band was found in the reaction of CP^{WT} (Fig. 8A). After protein identification of the single band using LC-MS/MS, NbPI2 (NBOR2273), a *N. benthamiana* protein similar to a putative proteinase inhibitor of *N. glutinosa* (AAF15901) (Park et al. 2000), was identified (Table 2). A homologous gene, *NbPI1* (NBOR2375), was identified from the transcriptome database based on *NbPI2* sequence similarity, and both genes were up-regulated in ORSV-infected plants (Fig. 7C and D). This band was not observed in the input extracts of either CP, suggesting that it was enriched during the coimmunoprecipitation process. Furthermore, the results of the in vitro binding assay indicated that ORSV CP has a strong binding affinity to NbPI2 (Fig. 9D). However, a weak coimmunoprecipitation signal of NbPI1 was observed at longer exposure times (Fig. 9D), suggesting that ORSV CP prefers to bind NbPI2 rather than NbPI1.

Based on the results of the large-scale protein identification, the divalent 472.25 m/z peptide of NbPI2 was enriched in the CP^{E100A} sample on the extracted ion chromatogram (Fig. 8B, the bottom-right panel shows a peak at a retention time of 27.12 min for CP^{E100A}), whereas it was present in smaller amounts in the CP^{WT} sample and was absent in the mock control sample (Fig. 8B, the middle and upper right panels show a peak at a retention time of 27.30 min for CP^{WT} and none for mock sample), indicating that NbPI2 is associated with ORSV

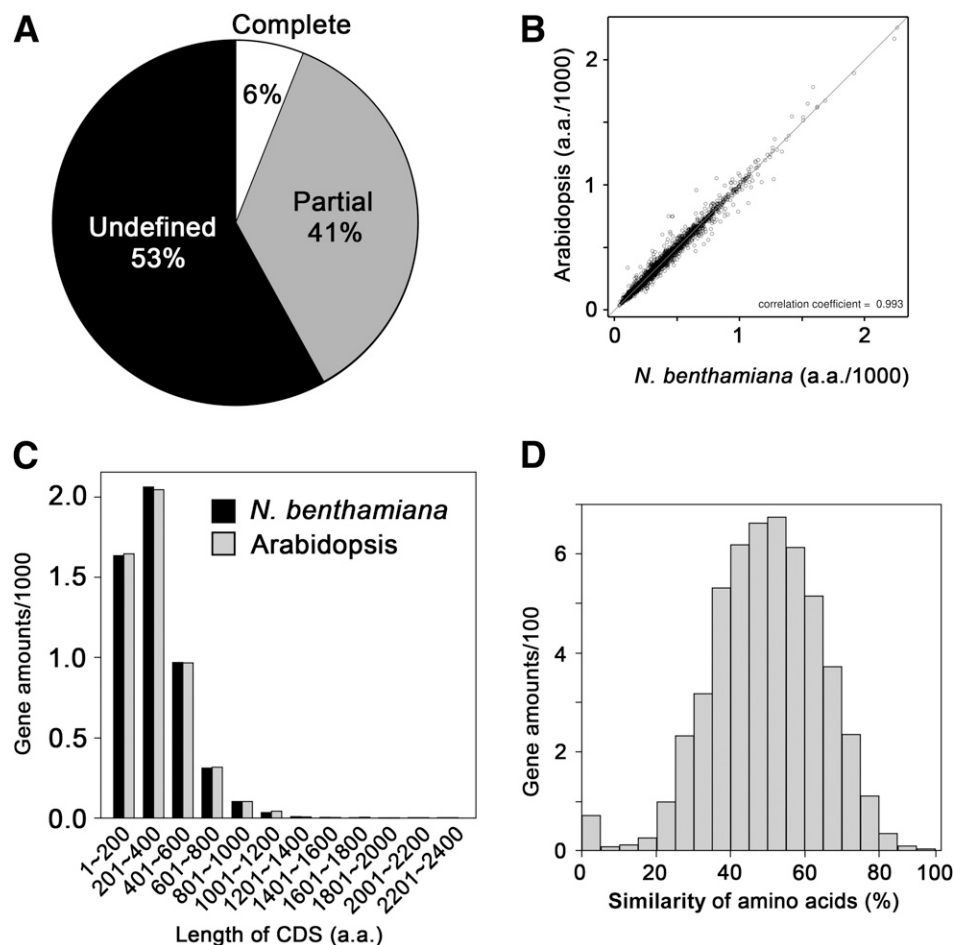


Fig. 6. Statistical analysis of gene similarity between *Nicotiana benthamiana* and *Arabidopsis*. **A**, Pie chart shows the percentages of complete genes, partial genes, and undefined contigs. **B**, Scatter plot of the coding sequence (CDS) lengths of *N. benthamiana* versus those of *Arabidopsis*. **C**, The length distribution comparison and **D**, amino acid similarity of the CDS of *Arabidopsis* and *N. benthamiana* are shown.

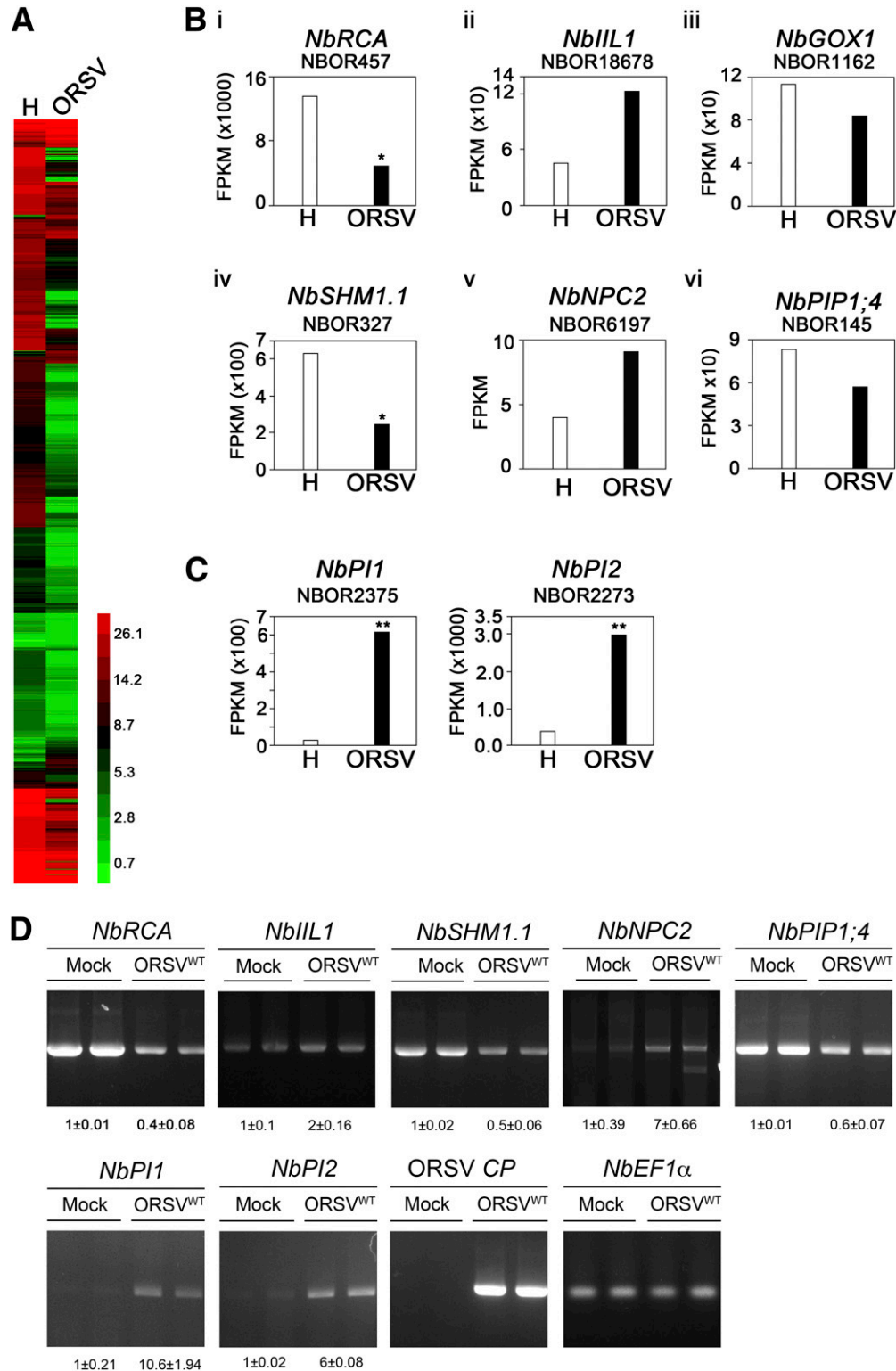


Fig. 7. Comparison of the gene expression patterns between healthy and *Odontoglossum ringspot virus* wild type (ORSV^{WT})-infected *Nicotiana benthamiana* plants using next-generation sequencing. **A**, The gene expression patterns of healthy and ORSV^{WT}-infected *N. benthamiana*. **B**, Comparison of the gene expression levels of ORSV CP^{WT}-interacting proteins (CP^{WT}-IP). The FPKM (fragments per kilobase of transcript per million mapped reads) value was used to indicate the gene expression levels in healthy and ORSV-infected *N. benthamiana*. **C**, *NbPI1* and *NbPI2* gene expression levels. The FPKM levels of ORSV-infected plants were significantly different from healthy plants, based on DESeq analysis. A single asterisk (*) indicates *P* value < 0.05, double asterisks (**) indicate *P* value < 0.01. **D**, The validation of CP^{WT}-IP gene expressions between mock- and ORSV-infected plants by semiquantitative reverse transcription-polymerase chain reaction. The *EF1α* gene served as an internal control. Numbers refer to the signal intensity of gene expression levels after normalization against the loading control (*n* = 3). The CP^{WT}-IP gene level in the mock sample was arbitrarily set as 1.0.

CP and especially with CP^{E100A}. The appearance of the divalent 493.25 m/z peptide of ORSV CP in both the CP^{WT} and CP^{E100A} samples (Fig. 8B, middle and bottom left panels) but not the mock controls also ensured that the coimmunoprecipitation and LC-MS/MS procedures were successful. These data confirmed the tight association between CP^{E100A} and NbPI2 of *N. benthamiana* in vivo.

To evaluate the association between NbPI2 and ORSV infection, we first examined the expression pattern of *NbPI2* in healthy and ORSV-infected plants. The results of a semi-quantitative RT-PCR analysis with *NbPI2* gene-specific primers showed that *NbPI2* mRNA was highly expressed in ORSV^{WT} and ORSV^{E100A}-infected *N. benthamiana* at 10 dpi compared with the healthy or mock-inoculated plants (Fig. 8C). A weaker signal was detected in mock-inoculated plants, which was most

likely because *NbPI2* was also induced by wounding (Fig. 8C), indicating that *NbPI2* is an ORSV- or wound-induced gene.

Knock-down of *NbPI1* and *NbPI2* by VIGS.

For the NbPI1 and NbPI2 functional assay, TRV-NbPI^c, which is *Tobacco rattle virus* containing the conserved sequences of *NbPI1* and *NbPI2*, was used for VIGS of *NbPI1* and *NbPI2* expression in *N. benthamiana* plants. The TRV-NbPI^c-infected plants did not induce *NbPI1* and *NbPI2* expression when infected with ORSV, whereas ORSV-infected or TRV + ORSV mix-infected plants had highly induced *NbPI1* and *NbPI2* expression (Fig. 10A),

Table 1. Significant gene ontology (GO) terms from the gene set enrichment analysis for the 12,135 genes that showed twofold differential expression during *Odontoglossum ringspot virus* (ORSV) infection (false discovery rate [FDR] ≤ 10⁻¹⁰)

GO accession	Type ^a	Term	FDR
GO:0009987	P	Cellular process	8.30E-40
GO:0009791	P	Postembryonic development	9.20E-38
GO:0008152	P	Metabolic process	6.70E-32
GO:0044237	P	Cellular metabolic process	7.80E-24
GO:0050896	P	Response to stimulus	1.00E-23
GO:0044238	P	Primary metabolic process	2.20E-22
GO:0032501	P	Multicellular organismal process	4.20E-20
GO:0007275	P	Multicellular organismal development	2.30E-19
GO:0051179	P	Localization	3.00E-18
GO:0051234	P	Establishment of localization	1.40E-17
GO:0032502	P	Developmental process	2.30E-17
GO:0006810	P	Transport	4.10E-17
GO:0048856	P	Anatomical structure development	9.20E-16
GO:0006950	P	Response to stress	5.30E-15
GO:0044262	P	Cellular carbohydrate metabolic process	2.20E-13
GO:0034641	P	Cellular nitrogen compound metabolic process	8.00E-13
GO:0009628	P	Response to abiotic stimulus	8.20E-13
GO:0042221	P	Response to chemical stimulus	1.40E-12
GO:0051716	P	Cellular response to stimulus	5.20E-12
GO:0003006	P	Reproductive developmental process	9.80E-11
GO:0033036	P	Macromolecule localization	1.60E-10
GO:0005623	C	Cell	1.10E-81
GO:0044464	C	Cell part	1.10E-81
GO:0005622	C	Intracellular	8.70E-67
GO:0044424	C	Intracellular part	2.10E-66
GO:0005737	C	Cytoplasm	1.80E-57
GO:0043229	C	Intracellular organelle	3.30E-56
GO:0043226	C	Organelle	3.30E-56
GO:0044444	C	Cytoplasmic part	2.00E-54
GO:0016020	C	Membrane	3.10E-52
GO:0043227	C	Membrane-bounded organelle	1.30E-48
GO:0043231	C	Intracellular membrane-bounded organelle	3.50E-48
GO:0005886	C	Plasma membrane	4.60E-39
GO:0044422	C	Organelle part	1.00E-23
GO:0044446	C	Intracellular organelle part	1.30E-23
GO:0032991	C	Macromolecular complex	2.40E-14
GO:0009536	C	Plastid	9.30E-14
GO:0043232	C	Intracellular non-membrane bounded organelle	1.50E-13
GO:0043228	C	Non-membrane bounded organelle	1.50E-13
GO:0043234	C	Protein complex	1.30E-12
GO:0005739	C	Mitochondrion	4.00E-12
GO:0005829	C	Cytosol	1.20E-11
GO:0009507	C	Chloroplast	1.20E-11
GO:0005634	C	Nucleus	4.50E-10

^a P = biological processes, C = cellular components, M = molecular functions.

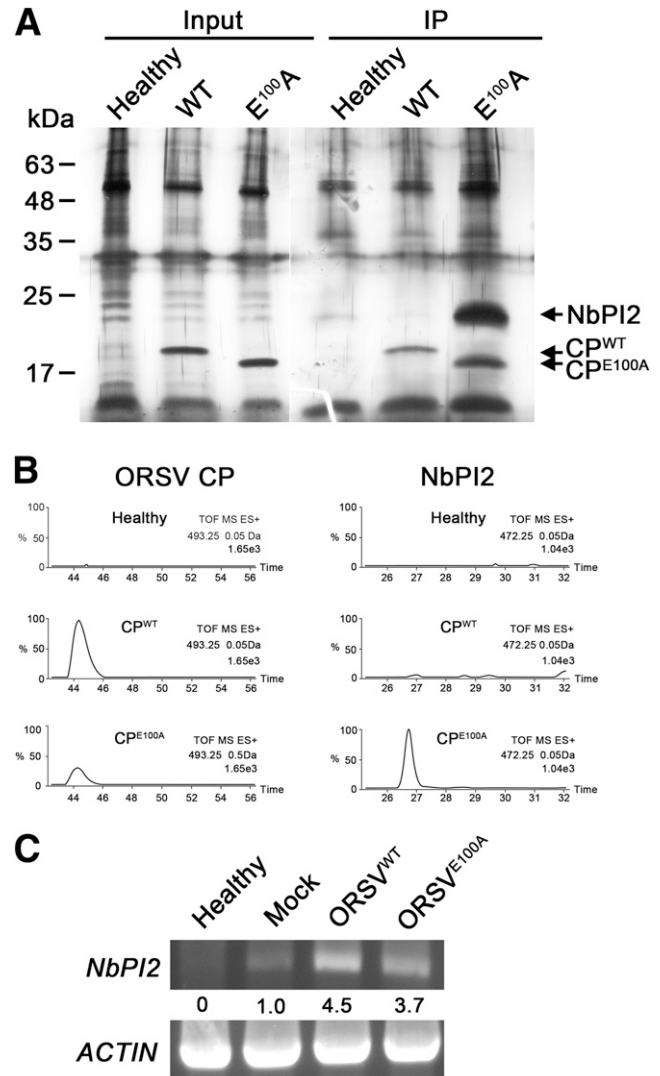


Fig. 8. Identification of *Odontoglossum ringspot virus* (ORSV) capsid protein-interacting host proteins (CP-IP) by coimmunoprecipitation. **A**, Silver staining of the coimmunoprecipitation products from the extracts of healthy, ORSV^{WT}- or ORSV^{E100A}-infected plants (right panel). The arrow indicates the NbPI2 protein, which is specifically associated with CP^{E100A}. The original plant extracts were also stained as input controls (left panel). **B**, Extracted ion chromatograms of ORSV CP ($m/z = 493.25$) (left panels) and NbPI2 ($m/z = 472.25$) (right panels). The horizontal axis represents the retention times in liquid chromatography, and the vertical axis indicates the signal intensity. **C**, Expression of the *NbPI2* gene was induced during ORSV infection. The semiquantitative reverse transcription-polymerase chain reaction of RNA from healthy, mock-, ORSV^{WT}-, and ORSV^{E100A}-inoculated *Nicotiana benthamiana* at 10 days postinoculation. The *ACTIN* gene served as an internal control. Numbers refer to signal intensity of *NbPI2* expression levels after normalization against the loading control. The *NbPI2* level in mock sample was arbitrarily set as 1.0.

suggesting that *NbPI1* and *NbPI2* were silenced by TRV-NbPI^c. However, the amount of ORSV did not significantly change in TRV-NbPI^c VIGS plants compared with TRV-infected plants (Fig. 10B), suggesting that the loss-of-function of NbPI1 and NbPI2 did not interfere with ORSV infection. However, we cannot exclude the synergistic effects produced by TRV and ORSV coinfection in the same plants because they resulted in the high amounts of ORSV in TRV-NbPI^c VIGS plants. In summary, these data indicated that *NbPI1* and *NbPI2* might be involved in the plant defense response against ORSV infection. Determining the precise function of NbPI1 and NbPI2, however, will require further investigation.

DISCUSSION

E¹⁰⁰ is essential for the CP-CP interaction in particle assembly.

In this study, we created an ORSV^{E100A} mutant virus that lost its systemic movement ability in *N. benthamiana*, and this virus

also contained a distinct *MscI* RFLP marker and a unique CP^{E100A} size. The E¹⁰⁰ residue of the ORSV CP is a conserved amino acid in the genus *Tobamovirus*, suggesting that the E¹⁰⁰ residue plays an important role in the virus life cycle. The data from ISEM and size-exclusion chromatography analyses revealed the defective assembly of viral particles in ORSV^{E100A}, indicating that an intact virus particle is necessary for ORSV systemic movement. This finding is consistent with previous studies in which the encapsidation of tobamoviruses was shown to be important for viral systemic movement (Dawson et al. 1988; Saito et al. 1990; Siegel et al. 1962; Takamatsu et al. 1987). In addition, the CP^{WT}-CP^{WT} self-interaction is much stronger than the CP^{WT}-CP^{E100A} or CP^{E100A}-CP^{E100A} interaction. In TMV, the CP^{T42W} mutant showed an altered CP-CP interaction, which resulted in the abnormal aggregation of virus particles in vivo (Bendahmane et al. 1997). Therefore, the E¹⁰⁰ residue of the ORSV CP might affect the structure of viral particles by changing the CP-CP interaction affinity.

Table 2. Wild-type capsid protein (CP^{WT})- and CP^{E100A}-interacting proteins

Gene	Contigs ID ^a	Ref ID ^b	Description	Score ^c		Mass (Da) ^d	FPKM ^e	
				WT	E ^{100A}		Mock	ORSV
<i>NbPSAE2</i>	NBOR690	AT2G20260	Photosystem I subunit E-2	46	33	14782	2064.2	1859.0
<i>NbGRF5</i>	NBOR9061	AT5G16050	GRF5	22	39	29526	56	80
<i>NbPI2</i>	NBOR2273	ABX76298	Kunitz family trypsin and protease inhibitor protein	64	181	26843	394	2975
<i>NbRBCS1A.1</i>	NBOR92	AT1G67090	Rubisco small subunit 1A	52	30	15623	14465	12930
<i>NbRBCS1A.2</i>	NBOR58			65	N/A	9774	5855	2414
<i>NbPSAF.1</i>	NBOR390	AT1G31330	Photosystem I subunit F	25	N/A	9719	1477	651
<i>NbPSAF.2</i>	NBOR392			N/A	39	2655		
<i>NbPSAD1</i>	NBOR676	AT4G02770	Photosystem I subunit D-1	23	44	22471	1971	1683

^a The transcriptome contig of the *Nicotiana benthamiana* sequence identification number.

^b The *Arabidopsis* Genome Initiative and European Molecular Biology Laboratory reference identification numbers.

^c The liquid chromatography-tandem mass spectrometry score.

^d The mass of the identified peptide

^e Fragments per kilobase of transcript per million mapped reads (FPKM) of transcriptome from the healthy plants (mock) and from *Odontoglossum ringspot virus* (ORSV)-infected plants.

Table 3. *Odontoglossum ringspot virus* wild-type interacting capsid proteins (ORSV-CP^{WT}) that were identified by MASCOT, using the ContigViews *Nicotiana benthamiana* database

Gene	Contigs ID ^a	Ref ID ^b	Description	Score ^c		Mass (Da) ^d	FPKM ^e	
				WT	E ^{100A}		Mock	ORSV
<i>NbFIB4</i>	NBOR6354	AT3G23400	FIBRILLIN 4	35	N/A	14845	211.7	291.5
<i>NbGOX1</i>	NBOR1162	AT3G14420	Glycolate oxidase 1	35	N/A	21998	113	83
<i>NbSHM1.1</i>	NBOR327	AT4G37930	Serine transhydroxymethyltransferase 1	31	N/A	19214	633	245
<i>NbCNGC1</i>	NBOR12131	AT5G53130	Cyclic nucleotide gated channel 1	21	N/A	75186	15	42
<i>NbPIPI;4</i>	NBOR145	AT4G00430	Plasma membrane intrinsic protein 1;4	22	N/A	12145	83	57
<i>NbFLN1</i>	NBOR16452	AT3G54090	FRUCTOKINASE-LIKE 1	30	N/A	55196	26	43
<i>NbIIL1</i>	NBOR18678	AT4G13430	Isopropyl malate isomerase large subunit 1	21	N/A	19023	46	123
<i>NbIBS1</i>	NBOR22975	AT1G18670	Impaired in baba-induced sterility 1	42	N/A	77365	7	12
<i>NbAGT1</i>	NBOR316	AT2G13360	Alanine:glyoxylate aminotransferase	40	N/A	22684	1325	471
<i>NbORC2</i>	NBOR45173	AT2G37560	Origin recognition complex second largest subunit 2	20	N/A	9810	9	18
<i>NbRCA</i>	NBOR457	AT2G39730	Rubisco activase	26	N/A	15745	13481	4900
<i>NbVCL1</i>	NBOR48019	AT2G38020	Vacuoleless 1	25	N/A	8655	4	2
<i>NbSK21</i>	NBOR4906	AT3G61415	SKP1-like 21	26	N/A	40372	24	21
<i>NbNPC2</i>	NBOR6197	AT2G26870	Nonspecific phospholipase C2	33	N/A	11207	4	9
NA ^f	NBOR6246	AT3G24880	Helicase/SANT-associated DNA binding protein	31	N/A	102850	4	4

^a Sequence identification number from the transcriptome contig of *N. benthamiana*.

^b The *Arabidopsis* Genome Initiative reference identification number.

^c The liquid chromatography-tandem mass spectrometry score.

^d The mass of the identified peptide

^e Fragments per kilobase of transcript per million mapped reads (FPKM) of transcriptome from the healthy plants (mock) and from *Odontoglossum ringspot virus* (ORSV)-infected plants.

^f Not available from its common name in The *Arabidopsis* Information Resource database.

The integrated omics approach and experimental validation for improving protein identification.

Traditional proteomics analysis uses the National Center for Biotechnology Information nonredundant (NCBI nr) database for protein identification. Currently, the high-throughput NGS technique provides an advantage for sequencing whole transcriptomes of nonmodel organisms, using a de novo assembly approach to bypass the requirement for genomic information (Liu et al. 2014). Through appropriate gene annotation, the integrated omics approach uses ORF information to provide a precise spectrum for protein identification. This organism-specific spectrum increases the accuracy of protein identification. Both the identification and expression of these IP can be evaluated using transcriptome assays. Therefore, the integrated

omics approach provides a comprehensive view of systems biology to understand the virus-host interaction.

High-throughput data must be validated by experimental approaches to confirm the effectiveness of the high-throughput strategy. Liu et al. (2014) used customized microarrays to verify transcript expressions in a nonmodel organism. To assess proteomes, gene cloning and soluble recombinant protein purification are limiting factors in the validation of protein-protein interactions. In this study, we used the pEXP5-CT/TOPO TA technology with the Expressway Cell-Free *E. coli* expression system to perform quickly cloning and recombinant protein expression in vitro. The candidate genes in the expression plasmid can be used to directly express the recombinant proteins by in vitro transcription and translation. The soluble

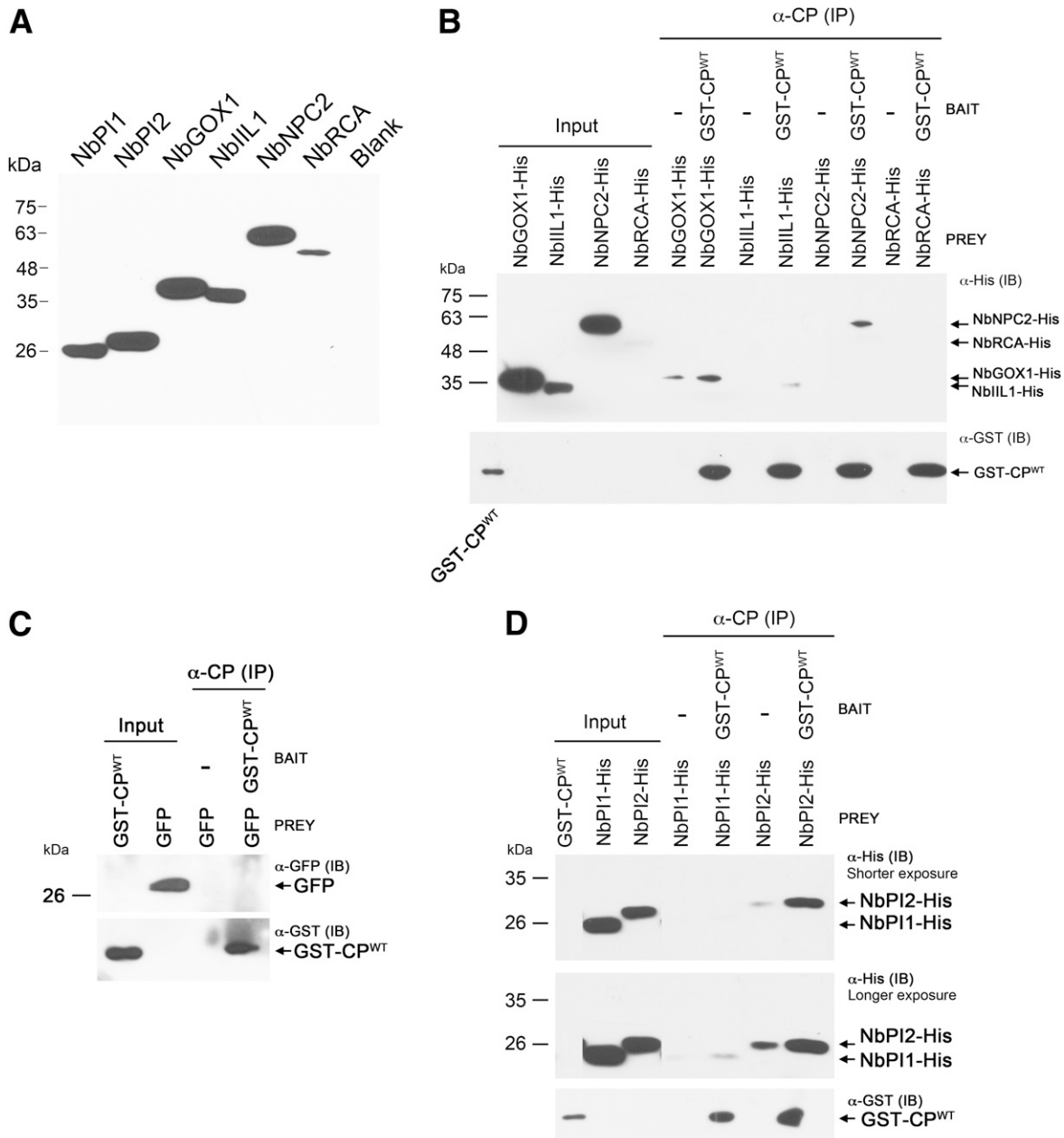


Fig. 9. Experimental validation of the physical interaction between *Odontoglossum ringspot virus* (ORSV) capsid protein (CP) and CP-interacting proteins CP-IP. **A**, In vitro transcribed or translated CP^{WT}-IP that fused with the His-tag were examined by Western blot analysis with an anti-His antibody. **B**, Evaluation of the protein-protein interaction between glutathione *S*-transferase (GST)-CP^{WT} and CP^{WT}-IP by coimmunoprecipitation. The GST-CP^{WT} was used as bait protein, whereas His-tag fused recombinant CP^{WT}-IP were used as prey. **C**, The coimmunoprecipitation of GST-CP^{WT} + GFP was used as a negative control. **D**, Evaluation of the protein-protein interaction between GST-CP^{WT} and NbPI1 and NbPI2 by coimmunoprecipitation.

recombinant proteins can be used as a prey for in vitro binding assay to validate high-throughput proteomic data. Moreover, VIGS provides an advantage by quickly knocking down the gene expression for loss-of-function assays. Thus, combining omics and experimental approaches has provided a new direction in functional genomic studies of nonmodel organisms.

Photosystem components aid in virus infection.

Many reports have indicated that several photosystem components are involved in virus infection (Li et al. 2008; Manfre et al. 2011; Pineda et al. 2010; Zhang et al. 2008). In ToMV, CP was shown to colocalize with the IP-L protein on chloroplast thylakoid membranes and caused chlorosis symptoms (Li et al. 2008; Zhang et al. 2008). In addition, chloroplast impairment increases the susceptibility of the plant to *Turnip mosaic virus* infection (Manfre et al. 2011). Moreover, protein related to photosynthesis pathways, such as the electron-transport chain and the Benson-Calvin cycle, have been shown to be decreased in virus-infected tissue (Pineda et al. 2010). These results indicated that viral proteins might control chloroplast function to aid virus infection. Our LC-MS/MS results are consistent with the observation that most of the CP-IP were plant photosystem subunits, e.g., NbPSAE2, NbPSAF.1, NbPSAF.2, and NbPSAD1. One of the CP^{WT}-IP, NbIIL1, was highly expressed in ORSV-infected plants. AtIIL1 (AT4G13430) is a chloroplast-localized protein, and the expression levels of *AtIIL1* affect leaf development (Sureshkumar et al. 2009; Zybailov et al. 2008). AtRCA (AT2G39730) is ancillary to CO₂ fixation by Rubisco in photosynthesis (Boex-Fontvieille et al. 2014; Portis 2003), whereas the CP^{WT}-interacting *NbRCA* was down-regulated in ORSV-infected plants. We suggest that CP targets and interacts

with chloroplast proteins to control chloroplast function during virus infection, replication, or movement.

CP^{WT}-specific IP in response to stresses and DNA replication.

The putative role of the nonspecific phospholipases C of *Arabidopsis* in signal transduction of the plant defense system may be attributable to diacylglycerols that generate reactive oxygen species (ROS) (Pokotylo et al. 2013; Scherer et al. 2002; Yamaguchi et al. 2005). Furthermore, AtGOX1 and AtSHM1.1 also control ROS production in *Arabidopsis* (Chern et al. 2013; Fahnenstich et al. 2008; Zhou et al. 2012). In addition, the plasma membrane intrinsic protein of *Arabidopsis* (AtPIP) is a type of aquaporin that controls transmembrane water flow to overcome chilling tolerance (Lee et al. 2012). The AtPIP1;4 aquaporin was up-regulated in roots exposed to low air temperatures (Jang et al. 2004). In the transcriptome data, *NbGOX1*, *NbSHM1.1*, and *NbPIP1;4* were down-regulated following ORSV infection, whereas *NbNPC2* was up-regulated in ORSV-infected plants, suggesting that the two forces from virus and host counteract each other.

Moreover, the expression levels of *NbFLN1* and *NbORC2* were induced by ORSV infection, and both proteins interact with ORSV CP^{WT} (Supplementary Fig. 2). The *Arabidopsis* ortholog of AtFLN1 is involved in the function of the plastid-encoded RNA polymerase in the transcriptionally active chromosomes of chloroplasts (Gilkerson et al. 2012). Furthermore, the *Arabidopsis* origin recognition complex (ORC) is composed of six subunits that form a prereplication complex (pre-RC) in endoreplicating cells (Diaz-Trivino et al. 2005). The pre-RC facilitates the formation of DNA replication complexes, resulting in DNA polymerase and other accessory factors to provide access to the activated origins of replicating DNA (Bell and Dutta 2002). Therefore, we hypothesize that ORSV CP^{WT} might interfere with gene expression in chloroplasts and disrupt cell division. Because these genes are components of the nuclear complex, we cannot exclude the possibility that ORSV might recruit these components for viral replication.

NbPI1 and NbPI2 might play a role in plant immunity.

The Kunitz type of proteinase inhibitor gene of *N. glutinosa* (*NgPI*) has been shown to be highly induced in a TMV-infected susceptible variety (SR1) and a resistant variety (*N. tabacum* cv. Xanthi nc) (Park et al. 2000). The rapid and transient accumulation of *NgPI* within 24 h of TMV infection implies that *NgPI* is involved in a signaling process that leads to defense responses (Park et al. 2000). The ortholog of *NgPI* in *Arabidopsis*, *AtPI* (AT1G17860), was shown to be up-regulated in response to stress and geminivirus infection (Ascencio-Ibáñez et al. 2008; dit Frey et al. 2010). In *N. benthamiana*, two homologous genes, *NbPI1* and *NbPI2*, were highly induced in ORSV-infected plants, but only NbPI2 had high binding affinity with ORSV CP. Furthermore, our mass spectrometry data indicated that CP^{E100A} has a stronger interaction with NbPI2 than CP^{WT}-NbPI2. NbPI2 did not evolve a strong interaction with CP^{E100A} via natural selection because the CP is a laboratory-created mutant. Our explanation for this phenomenon is that the substitution (E¹⁰⁰A) on CP resulted in a strong interaction with NbPI2 and that the NbPI2-CP interaction prevents viral particle assembly or prevents the systemic movement of the virus. However, the synergistic effect of coinfection resulted in an absence of differences in ORSV amounts between TRV and TRV-NbPI^c VIGS plants. Stable *NbPI* RNAi transgenic plants might provide better evidence to determine whether both NbPI are important in host defense or in ORSV infection.

In conclusion, we demonstrated that viral particle assembly is associated with ORSV systemic movement in *N. benthamiana*.

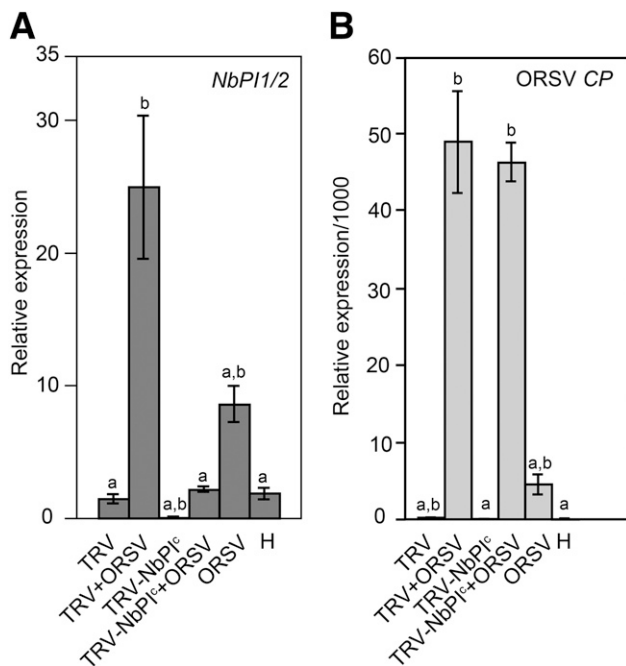


Fig. 10. Evaluation the *Odontoglossum ringspot virus* (ORSV) infectivity on *NbPI1/2* VIGS plants. **A**, The relative expression levels of *NbPI1* and *NbPI2* and **B**, ORSV CP on plants inoculated by various *Tobacco rattle virus* (TRV) constructs and then challenged by ORSV were detected by real-time reverse transcription-polymerase chain reaction. The bars represent standard errors ($n = 14$). Relative expression levels were normalized with the *NbEF1 α* level. "H" indicates the healthy plants. Relative expression levels were significantly different (P values < 0.01) from those of TRV+ORSV or H plants in each RNA sample, based on a Student's t test. The letter a indicates differentially expressed (DE) to TRV+ORSV and b indicates DE to H plants.

Several CP-IP were identified using an integrated omics and experimental approach, which suggested several new research directions to further elucidate the systemic movement of ORSV and its interactions with the host plant. Finally, whether NbPI1 and NbPI2 play important roles in plant immunity requires further investigation.

MATERIALS AND METHODS

Tobamovirus CP sequence analysis and protein structure prediction.

The CP sequences of ORSV and other tobamoviruses were obtained from GenBank. The sequence comparison was performed using the Align X program of the Vector NTI Suit 10.0 (Invitrogen). The amino acid sequence of ORSV CP was investigated using the Protein Structure Prediction Server (Chen et al. 2006) for protein structure prediction. The results of the prediction were further refined using PyMOL.

Construction of infectious clones and protein expression clones.

To construct the single amino acid mutation E¹⁰⁰A of ORSV CP, pET29a(+)-ORCP (Lee and Chang 2008) containing the ORSV CP^{WT} gene was mutated by PCR-mediated site-directed mutagenesis with the following set of primers, mORCPF (5'-GAATAATCGAGGTGGCCAATCCGCAGAAT-3') and mORCPR (5'-ATTCTGCGGATTGGCCACCTCGATTATTC-3') (bold indicates the point mutation site; underlining indicates the *MscI* restriction enzyme site). The amplicon was used to replace the CP gene of the full-length infectious clone pORSV^{WT} (Lee 2008) to generate pORSV^{E100A}.

For protein expression, the 6×His-tagged CP^{E100A} gene was cloned into pET29a(+) (Novagen) to generate pET29-CP^{E100A}. The GST-tagged CP^{WT} and CP^{E100A} genes were cloned into pGEX-4T-1 (GE Healthcare) to generate pGEX-CP^{WT} and pGEX-CP^{E100A}, respectively.

Plant materials and virus inoculation.

ORSV *in vitro* infectious clones harboring a wild-type genome (pORSV^{WT}) or a mutant CP gene (pORSV^{E100A}) were expressed from a T7 promoter. For plant inoculation, capped RNA transcripts were generated by T7 RNA polymerase (New England BioLabs) and were inoculated on fully expanded leaves of *N. benthamiana* or *C. quinoa* (0.3 to 0.5 μg of transcript RNAs per leaf). The inoculated plants were housed in the greenhouse with a 16-h light period.

RNA extraction, RT-PCR, and RNA deep-sequencing analysis.

The plant total RNA extraction miniprep system (Viogene) was used for the preparation of plant total RNA. The ORCP-F1 and ORCP-R1 primers were used for RT-PCR analysis of the ORSV CP gene (Lee and Chang 2006). *MscI* digestion (New England BioLabs) was performed to discriminate ORSV^{E100A} from ORSV^{WT}. The PCR products and the digested products were analyzed by 1.5% agarose gel electrophoresis. For RNA deep sequencing, total RNA was prepared from healthy or 10-dpi ORSV^{WT}-infected *N. benthamiana* plants, according to the manufacturer's instructions. Deep sequencing was performed using an Illumina HiSeq 2000 instrument (Genomics BioSci & Tech Co.). The transcriptomes were obtained using the *de novo* assembler in CLC Genomics Workbench 5.1 (CLC bio). The transcriptome expression profiles and database are available on the ContigViews web server. Name-calling and ORF annotations were determined using the rule-based predictor of ContigViews. The FPKM were calculated using Bowtie2 and eXpress-D software (Langmead and Salzberg 2012; Roberts

et al. 2013). Differential expression analysis between healthy and ORSV^{WT}-infected plants was performed with BioConductor (Gentleman et al. 2004) and the DESeq2 package (Love et al. 2014). Gene set enrichment analysis for annotated contigs with at least twofold change of expressions between healthy and ORSV^{WT}-infected plants was accomplished by agriGO toolkit (Du et al. 2010).

Western blot analysis.

Protein samples were extracted with 10 mM sodium phosphate buffer (pH 7.2), were separated in a 12.5% sodium dodecyl sulfate (SDS)-polyacrylamide gel electrophoresis mini-gel and transferred to polyvinylidene difluoride membranes (GE Healthcare). Western blot analysis was conducted with rabbit anti-ORSV CP antiserum (Lee and Chang 2008), an anti-His polyclonal antibody (LTK BioLaboratories), or an anti-GST polyclonal antibody (LTK BioLaboratories). Gels or membranes were stained with Coomassie brilliant blue R250, and the expression level of Rubisco was used as a loading control.

ISEM.

A carbon-coated Formvar copper grid (200 mesh) was incubated with an anti-ORSV CP antibody solution that was diluted in 10 mM sodium phosphate buffer (pH 7.2) for 15 min at room temperature. The antibody-coated grid was incubated with a virion solution derived from leaf extracts prepared in 10 volumes of (vol/wt) 10 mM sodium phosphate buffer (pH 7.2) and were centrifuged at 10,000 rpm (Eppendorf Centrifuge 5424) for 3 min to discard the cell debris. The grid was further incubated with an anti-ORSV CP antibody for 15 min at room temperature. Excess liquid was carefully removed from the edge of the grid, using a deckle-edged paper. Two percent phosphotungstic acid (pH 7.0) was dripped onto the semidry grid, and the sample was negative stained for 1 min. The liquid was removed using deckle-edged paper, and the grid was allowed to air dry for at least 2 days before observation through a transmission electron microscope. Photographs were taken at a magnification of 80,000, and the size of the viral particle was calculated using the detector on the real-time images.

Size-exclusion chromatography.

Plant tissues were homogenized in 2 to 4 volumes of extraction buffer (200 mM Tris-HCl, pH 7.4, 150 mM NaCl, 5 mM dithiothreitol [DTT], protease inhibitor cocktail [Roche Applied Science] and proteasome inhibitor set II [Calbiochem]) and were centrifuged twice at 10,000 rpm (Eppendorf Centrifuge 5424) for 10 min at 4°C to remove the cell debris. The plant extracts were loaded onto a HiPrep 16/60 Sephacryl S-200 HR column (GE Healthcare), using the AKTA Explorer Fast protein liquid chromatography (FPLC) system. The FPLC system was run at a constant flow rate at 0.5 ml/min and fractions were collected every 2 ml. A 10-μl aliquot of each fraction was analyzed by Western blot analysis with anti-ORSV CP antiserum. The excess unloading plant extract was saved as input control, and additional FPLC runs with given size markers were conducted to mark the relative sizes of the FPLC fractions.

In vitro CP-CP interaction assay.

Protein coprecipitation was performed by incubating GST, GST-CP^{WT}, or GST-CP^{E100A} with CP^{WT}-His or CP^{E100A}-His in coprecipitation buffer (50 mM Tris, pH 7.5, 100 mM NaCl, 1 mM EDTA, 3 mM DTT plus 0.25, 0.5, or 1% Triton X-100) at 4°C for 1 h. PureProteome nickel magnetic beads (Millipore) were added at 4°C for 1 h to capture the target proteins. A magnetic stand for a 0.2-ml tube (DYNAL MPC-9600; Invitrogen) was used to pull down the magnetic protein complex. After five washes with coprecipitation buffer, the pulled-down

product was resuspended in 2× sample buffer (2% SDS, 10% glycerol, 1% β-mercaptoethanol, 0.005% bromophenol blue, 50 mM Tris-HCl, pH 6.8), was boiled at 96°C for 10 min, and was loaded onto a 12% SDS polyacrylamide gel. Western blot analysis was performed with an anti-GST polyclonal antibody to detect the existence of the GST fusion protein.

Coimmunoprecipitation and LC-MS/MS identification.

The Pierce crosslink immunoprecipitation kit (Thermo Scientific) was used to pull down the protein complex with affinity-purified anti-ORSV CP immunoglobulin G. After SDS-polyacrylamide gel electrophoresis, silver staining was performed. In brief, the gel was fixed overnight in fixing solution (50% methanol, 10% acetic acid, 0.05% formalin), was washed twice in 35% ethanol for 20 min for each wash, was sensitized in 0.02% Na₂S₂O₃ for 2 min, and finally, was washed in double-distilled (dd)H₂O three times for 5 min each. The gel was stained with staining solution (0.2% AgNO₃ and 0.076% formalin) for 30 min and was washed in ddH₂O for 1 min. Finally, the silver color was developed in developing solution (6% Na₂CO₃, 0.05% formalin, and 0.0004% Na₂S₂O₃) for approximately 1 min. All incubations were performed at room temperature.

Coomassie blue staining was used instead of silver staining to decrease the incompatibility of the LC-MS/MS analysis. The gel pieces were destained with 25 mM ammonium bicarbonate (ABC) and 50% acetonitrile, were reduced with 10 mM DTT and 25 mM ABC at 56°C for 1 h, and were alkylated with 55 mM iodoacetamide and 25 mM ABC at room temperature for 45 min. Trypsin (Promega) was used to digest the proteins into peptides at 37°C for 16 h (trypsin/total proteins = 1:50). The extracted peptides were desalted using C18 ZipTIP (Millipore) prior to LC-MS/MS analysis. The LC-MC/MC analyses were performed using a quadrupole time-of-flight mass spectrometer (Synapt G1; Waters) coupled with a nano ultrahigh performance liquid chromatography (nanoUHPLC) system (nanoACQUITY; Waters) and a tunnel frit nanoUHPLC column, as described in a previous study (Chen et al. 2012). The acquired MS/MS spectra were processed by UniQua (Chang et al. 2013), using the SynaptG1 preset parameter to obtain a fragment monoisotopic peak list, and were searched against the ContigViews *N. benthamiana* transcriptome database and NCBI nr protein database, using the MASCOT algorithm (Matrix Science) with previously described search parameters (Chen et al. 2010).

The proteins that were identified in the healthy sample were subtracted from the list of CP^{WT}- and CP^{E100A}-IP. The detailed identification scores of the CP^{WT} and CP^{E100A}-IP are listed in Supplementary Table 3.

In vitro transcription and translation for rapid validation of protein interaction.

The CP^{WT}-IP genes were amplified by RT-PCR with *Taq* DNA polymerase (Ampliqon) to obtain an extra “A” at the 3' ends for TA cloning. The primers used for RT-PCR are listed in Supplementary Table 4. The pEXP5-CT/TOPO TA expression kit (Invitrogen) was used for cloning CP^{WT}-IP genes, which were fused with a 6×His-Tag at the C-terminus of the recombinant protein. One microgram of the plasmid was used for in vitro cell-free transcription or translation for the recombinant protein production by Expressway Cell-Free *E. coli* expression system (Invitrogen). Each 5 μl of lysate containing CP-IP recombinant protein was incubated with 2 μg of GST-CP^{WT} recombinant protein in coprecipitation buffer (50 mM Tris, pH 7.5, 100 mM NaCl, 0.2% glycerol, 0.6% Triton X-100, and 0.5 mM β-mercaptoethanol) at room temperature for 1 h and was then applied with 10 μg of anti-ORSV CP polyclonal immunoglobulins and 30 μl of balanced suspension of Protein G PLUS-agarose beads

(Santa Cruz Biotechnology) for protein-capturing at room temperature for another 1 h. The protein-captured beads were washed twice with wash buffer (50 mM Tris, pH 7.5, 100 mM NaCl, 0.6% Triton X-100). Final precipitant was suspended in 20 μl of 2× sample buffer (2% SDS, 10% glycerol, 1% β-mercaptoethanol, 0.005% bromophenol blue, 50 mM Tris-HCl, pH 6.8) and was analyzed by Western blot for prey detection with anti-His (C-term)-horseradish peroxidase antibody (Invitrogen) or anti-GFP monoclonal antibody (GeneTex). The captured bait was measured by anti-GST monoclonal antibody (Bioss Scientific).

VIGS for *NbP11* and *NbP12*.

The 485-bp coding region (30 to 514 bp) of *NbP12* was amplified with NbP1VIGSF1 and NbP1VIGSR1 primers by RT-PCR because the region is highly conserved with *NbP11*. The RT-PCR product was cloned into pCR8/GW/TOPO vector (Invitrogen) to generate pCR8-TOPO-NBPI. The 485-bp fragment of *NbP12* (*NbP12*^c) was transferred into the TRV2-pYL279 plasmid (Liu et al. 2002) by a Gateway recombination system (Invitrogen) to generate pTRV2-NbP1^c. *Agrobacterium tumefaciens* (strain GV3101) was used to express pTRV1 (TRV RNA1) and pTRV2-NbP1^c following agroinfiltration to generate the TRV-NbP1^c virus in *N. benthamiana* plants for virus inoculum. TRV was used as a negative control.

For VIGS of *NbP11* and *NbP12*, the 3-week-old *N. benthamiana* plant was used and the first to fifth leaves (counted from the base) were used for TRV-NbP1^c inoculation. After 7 dpi, *NbP11/2*-VIGS plants were challenged with ORSV on the seventh and eighth leaves by mechanical inoculation. After 7 days of ORSV challenging inoculation, the twelfth and thirteenth leaves were collected for RNA extraction with the plant total RNA isolation kit (Viogene). Reverse transcription was performed using the SuperScript III first-strand synthesis system (Invitrogen) with oligo-dT and ORSV CP-specific reverse primers. *NbP11* and *NbP12* expression were evaluated for VIGS efficiency by detecting the conserved region with real-time RT-PCR, using a LightCycler 480 instrument (Roche). In addition, the ORSV CP RNA amounts were evaluated by real-time RT-PCR. The *NbEF1α* level was used as internal control. The *NbP1*, *ORSV CP*, and *NbEF1α* transcripts were quantified via a relative cycle threshold (Ct) method. All of the experiments were performed with three independent replicates to compensate possible loading errors. The relative expression levels were calculated based on the ΔΔCt value, and each sample was normalized according to the expression level of *NbEF1α*.

ACKNOWLEDGMENTS

This work was supported by grants from the Ministry of Science and Technology, Taiwan (NSC-102-2313-B-002-068-MY3 and NSC-102-2313-B-002-066-B-MY3) to S.-S. Lin. and (NSC99-2313-B-002-043-MY3) to Y.-C. Chang. S.-S. Lin and Y.-C. Chang designed the research methods. P.-C. Lin, W.-C. Hu, S.-C. Lee, and P.-Y. Chen performed the experiments. Y.-R. Chen designed the proteomics workflow. Y.-L. Chen, and C.-Y. Lee performed the proteomics analysis and data analysis. L.-Y. Liu performed the statistical assays on the deep sequence data. All of the authors discussed the results and commented on the manuscript, which was written by P.-C. Lin, Y.-C. Chang, and S.-S. Lin.

LITERATURE CITED

- Adams, M. J., Antoniw, J. F., and Kreuze, J. 2009. Virgaviridae: A new family of rod-shaped plant viruses. *Arch. Virol.* 154:1967-1972.
- Ascencio-Ibáñez, J. T., Sozzani, R., Lee, T. J., Chu, T. M., Wolfinger, R. D., Cella, R., and Hanley-Bowdoin, L. 2008. Global analysis of Arabidopsis gene expression uncovers a complex array of changes impacting pathogen response and cell cycle during geminivirus infection. *Plant Physiol.* 148: 436-454.

- Bell, S. P., and Dutta, A. 2002. DNA replication in eukaryotic cells. *Annu. Rev. Biochem.* 71:333-374.
- Bendahmane, M., Fitchen, J. H., Zhang, G., and Beachy, R. N. 1997. Studies of coat protein-mediated resistance to *Tobacco mosaic tobamovirus*: Correlation between assembly of mutant coat proteins and resistance. *J. Virol.* 71:7942-7950.
- Boex-Fontvieille, E., Davenport, M., Jossier, M., Hodges, M., Zivy, M., and Tcherkez, G. 2014. Phosphorylation pattern of Rubisco activase in *Arabidopsis* leaves. *Plant Biol Stuttg* 16:550-557.
- Chang, W. H., Lee, C. Y., Lin, C. Y., Chen, W. Y., Chen, M. C., Tzou, W. S., and Chen, Y. R. 2013. UniQua: A universal signal processor for MS-based qualitative and quantitative proteomics applications. *Anal. Chem.* 85:890-897.
- Chen, M. H., and Citovsky, V. 2003. Systemic movement of a tobamovirus requires host cell pectin methyltransferase. *Plant J.* 35:386-392.
- Chen, M. H., Sheng, J., Hind, G., Handa, A. K., and Citovsky, V. 2000. Interaction between the *Tobacco mosaic virus* movement protein and host cell pectin methyltransferase is required for viral cell-to-cell movement. *EMBO (Eur. Mol. Biol. Organ.) J.* 19:913-920.
- Chen, C. C., Hwang, J. K., and Yang, J. M. 2006. (PS)2: Protein structure prediction server. *Nucleic Acids Res.* 34:W152-W157.
- Chen, C. J., Tseng, M. C., Lin, H. J., Lin, T. W., and Chen, Y. R. 2010. Visual indicator for surfactant abundance in MS-based membrane and general proteomics applications. *Anal. Chem.* 82:8283-8290.
- Chen, C. J., Chen, W. Y., Tseng, M. C., and Chen, Y. R. 2012. Tunnel frit: A nonmetallic in-capillary frit for nanoflow ultra high-performance liquid chromatography-mass spectrometry applications. *Anal. Chem.* 84:297-303.
- Chern, M., Bai, W., Chen, X., Canlas, P. E., and Ronald, P. C. 2013. Reduced expression of glycolate oxidase leads to enhanced disease resistance in rice. *PeerJ* 1:e28.
- Dawson, W. O., Bublrick, P., and Grantham, G. L. 1988. Modifications of the *Tobacco mosaic virus* coat protein gene affecting replication, movement, and symptomatology. *Phytopathology* 78:783-789.
- Diaz-Trivino, S., del Mar Castellano, M., de la Paz Sanchez, M., Ramirez-Parra, E., Desvoves, B., and Gutierrez, C. 2005. The genes encoding *Arabidopsis* ORC subunits are E2F targets and the two *ORC1* genes are differentially expressed in proliferating and endoreplicating cells. *Nucleic Acids Res.* 33:5404-5414.
- dit Frey, N. F., Muller, P., Jammes, F., Kizis, D., Leung, J., Perrot-Rechenmann, C., and Bianchi, M. W. 2010. The RNA binding protein Tudor-SN is essential for stress tolerance and stabilizes levels of stress-responsive mRNAs encoding secreted proteins in *Arabidopsis*. *Plant Cell* 22:1575-1591.
- Du, Z., Zhou, X., Ling, Y., Zhang, Z., and Su, Z. 2010. agriGO: A GO analysis toolkit for the agricultural community. *Nucleic Acids Res.* 38: W64-W70.
- Fahnenstich, H., Scarpeci, T. E., Valle, E. M., Flügge, U. I., and Maurino, V. G. 2008. Generation of hydrogen peroxide in chloroplasts of *Arabidopsis* overexpressing glycolate oxidase as an inducible system to study oxidative stress. *Plant Physiol.* 148:719-729.
- Gentleman, R. C., Carey, V. J., Bates, D. M., Bolstad, B., Dettling, M., Dudoit, S., Ellis, B., Gautier, L., Ge, Y., Gentry, J., Hornik, K., Hothorn, T., Huber, W., Iacus, S., Irizarry, R., Leisch, F., Li, C., Maechler, M., Rossini, A. J., Sawitzki, G., Smith, C., Smyth, G., Tierney, L., Yang, J. Y., and Zhang, J. 2004. Bioconductor: Open software development for computational biology and bioinformatics. *Genome Biol.* 5:R80.
- Gilkerson, J., Perez-Ruiz, J. M., Chory, J., and Callis, J. 2012. The plastid-localized pfkB-type carbohydrate kinases FRUCTOKINASE-LIKE 1 and 2 are essential for growth and development of *Arabidopsis thaliana*. *BMC Plant Biol.* 12:102.
- Guarnieri, M. T., Nag, A., Smolinski, S. L., Darzins, A., Seibert, M., and Pienkos, P. T. 2011. Examination of triacylglycerol biosynthetic pathways via *de novo* transcriptomic and proteomic analyses in an unsequenced microalga. *PLoS ONE* 6:e25851.
- Hicks, G. R., Rojo, E., Hong, S., Carter, D. G., and Raikhel, N. V. 2004. Geminating pollen has tubular vacuoles, displays highly dynamic vacuole biogenesis, and requires VACUOLESS1 for proper function. *Plant Physiol.* 134:1227-1239.
- Hilf, M. E., and Dawson, W. O. 1993. The tobamovirus capsid protein functions as a host-specific determinant of long-distance movement. *Virology* 193:106-114.
- Holt, C. A., and Beachy, R. N. 1991. *In vivo* complementation of infectious transcripts from mutant *Tobacco mosaic virus* cDNAs in transgenic plants. *Virology* 181:109-117.
- Hong, Y., Shi, N. N., Xu, Y., Yang, K. F., Chen, Y., Wang, H. Z., and Xu, X. B. 2011. Development of a sensitive diagnostic assay to detect *Cymbidium mosaic virus* and *Odontoglossum ringspot virus* in members of the Orchidaceae. *J. Hortic. Sci. Biotechnol.* 86:69-73.
- Howe, E. A., Sinha, R., Schlauch, D., and Quackenbush, J. 2011. RNA-Seq analysis in MeV. *Bioinformatics* 27:3209-3210.
- Jang, J. Y., Kim, D. G., Kim, Y. O., Kim, J. S., and Kang, H. 2004. An expression analysis of a gene family encoding plasma membrane aquaporins in response to abiotic stresses in *Arabidopsis thaliana*. *Plant Mol. Biol.* 54:713-725.
- Karran, R. A., and Sanfaçon, H. 2014. Tomato ringspot virus coat protein binds to ARGONAUTE 1 and suppresses the translation repression of a reporter gene. *Mol. Plant Microbe Interact.* 27:933-943.
- Khenry, Y., Paradornuwat, A., Tantiwiwat, S., Phansiri, S., and Thaveechai, N. 2006. Incidence of *Cymbidium mosaic virus* and *Odontoglossum ringspot virus* in *Dendrobium* spp. in Thailand. *Crop Prot.* 25:926-932.
- Langmead, B., and Salzberg, S. L. 2012. Fast gapped-read alignment with Bowtie 2. *Nat. Methods* 9:357-359.
- Lee, S. C. 2008. Development of detection methods for two important orchid viruses, *Cymbidium mosaic virus* (CymMV) and *Odontoglossum ringspot virus* (ORSV), and construction and characterization of ORSV infectious cDNA clone. Ph.D. dissertation. Graduate Institute of Plant Pathology and Microbiology, National Taiwan University, Taipei.
- Lee, S. C., and Chang, Y. C. 2006. Multiplex RT-PCR detection of two orchid viruses with an internal control of plant nad5 mRNA. *Plant Path. Bulletin* 15:187-196.
- Lee, S. C., and Chang, Y. C. 2008. Performances and application of antisera produced by recombinant capsid proteins of *Cymbidium mosaic virus* and *Odontoglossum ringspot virus*. *Eur. J. Plant Pathol.* 122:297-306.
- Lee, S. H., Chung, G. C., Jang, J. Y., Ahn, S. J., and Zwiazek, J. J. 2012. Overexpression of PIP2;5 aquaporin alleviates effects of low root temperature on cell hydraulic conductivity and growth in *Arabidopsis*. *Plant Physiol.* 159:479-488.
- Li, Y., Wu, M. Y., Song, H. H., Hu, X., and Qiu, B. S. 2005. Identification of a tobacco protein interacting with tomato mosaic virus coat protein and facilitating long-distance movement of virus. *Arch. Virol.* 150: 1993-2008.
- Li, J., Brader, G., and Palva, E. T. 2008. Kunitz trypsin inhibitor: An antagonist of cell death triggered by phytopathogens and fumonisin b1 in *Arabidopsis*. *Mol. Plant* 1:482-495.
- Liu, Y., Schiff, M., and Dinesh-Kumar, S. P. 2002. Virus-induced gene silencing in tomato. *Plant J.* 31:777-786.
- Liu, L. Y., Tseng, H. I., Lin, C. P., Lin, Y. Y., Huang, Y. H., Huang, C. K., Chang, T. H., and Lin, S. S. 2014. High-throughput transcriptome analysis of the leafy flower transition of *Catharanthus roseus* induced by peanut witches'-broom phytoplasma infection. *Plant Cell Physiol.* 55: 942-957.
- Love, M. I., Huber, W., and Anders, S. 2014. Moderated estimation of fold change and dispersion for RNA-Seq data with DESeq2. *Genome Biol.* 15:550.
- Manfre, A., Glenn, M., Nuñez, A., Moreau, R. A., and Dardick, C. 2011. Light quantity and photosystem function mediate host susceptibility to *Turnip mosaic virus* via a salicylic acid-independent mechanism. *Mol. Plant Microbe Interact.* 24:315-327.
- Park, K. S., Cheong, J. J., Lee, S. J., Suh, M. C., and Choi, D. 2000. A novel proteinase inhibitor gene transiently induced by tobacco mosaic virus infection. *Biochim. Biophys. Acta* 1492:509-512.
- Pineda, M., Sajjani, C., and Barón, M. 2010. Changes induced by the *Pepper mild mottle tobamovirus* on the chloroplast proteome of *Nicotiana benthamiana*. *Photosynth. Res.* 103:31-45.
- Pokotylo, I., Pejchar, P., Potocký, M., Kocourková, D., Krčková, Z., Ruelland, E., Kravets, V., and Martinec, J. 2013. The plant non-specific phospholipase C gene family. Novel competitors in lipid signalling. *Prog. Lipid Res.* 52:62-79.
- Portis, A. R., Jr. 2003. Rubisco activase - Rubisco's catalytic chaperone. *Photosynth. Res.* 75:11-27.
- Rabindran, S., Robertson, C., Achor, D., German-Retana, S., A Holt, C., and Dawson, W. O. 2005. *Odontoglossum ringspot virus* host range restriction in *Nicotiana glauca* maps to the replicase gene. *Mol. Plant Pathol.* 6:439-447.
- Roberts, A., Feng, H., and Pachter, L. 2013. Fragment assignment in the cloud with eXpress-D. *BMC Bioinformatics* 14:358.
- Saito, T., Yamanaka, K., and Okada, Y. 1990. Long-distance movement and viral assembly of tobacco mosaic virus mutants. *Virology* 176:329-336.
- Scherer, G. F., Paul, R. U., Holk, A., and Martinec, J. 2002. Down-regulation by elicitors of phosphatidylcholine-hydrolyzing phospholipase C and up-regulation of phospholipase A in plant cells. *Biochem. Biophys. Res. Commun.* 293:766-770.
- Siegel, A., Zaitlin, M., and Sehgal, O. P. 1962. The isolation of defective tobacco mosaic virus strains. *Proc. Natl. Acad. Sci. USA* 48:1845-1851.
- Singh, D. K., Maximova, S. N., Jensen, P. J., Lehman, B. L., Ngugi, H. K., and McNellis, T. W. 2010. FIBRILLIN4 is required for plastoglobule

- development and stress resistance in apple and Arabidopsis. *Plant Physiol.* 154:1281-1293.
- Slaughter, A., Daniel, X., Flors, V., Luna, E., Hohn, B., and Mauch-Mani, B. 2012. Descendants of primed Arabidopsis plants exhibit resistance to biotic stress. *Plant Physiol.* 158:835-843.
- Su, C. L., Chao, Y. T., Alex Chang, Y. C., Chen, W. C., Chen, C. Y., Lee, A. Y., Hwa, K. T., and Shih, M. C. 2011. *De novo* assembly of expressed transcripts and global analysis of the *Phalaenopsis aphrodite* transcriptome. *Plant Cell Physiol.* 52:1501-1514.
- Sureshkumar, S., Todesco, M., Schneeberger, K., Harilal, R., Balasubramanian, S., and Weigel, D. 2009. A genetic defect caused by a triplet repeat expansion in *Arabidopsis thaliana*. *Science* 323:1060-1063.
- Takamatsu, N., Ishikawa, M., Meshi, T., and Okada, Y. 1987. Expression of bacterial chloramphenicol acetyltransferase gene in tobacco plants mediated by TMV-RNA. *EMBO (Eur. Mol. Biol. Organ.) J.* 6:307-311.
- Ueki, S., and Citovsky, V. 2002. The systemic movement of a tobamovirus is inhibited by a cadmium-ion-induced glycine-rich protein. *Nat. Cell Biol.* 4:478-486.
- Van Moerkercke, A., Fabris, M., Pöllier, J., Baart, G. J., Rombauts, S., Hasnain, G., Rischer, H., Memelink, J., Oksman-Caldentey, K. M., and Goossens, A. 2013. CathaCyc, a metabolic pathway database built from *Catharanthus roseus* RNA-Seq data. *Plant Cell Physiol.* 54:673-685.
- Wang, Y. F., Munemasa, S., Nishimura, N., Ren, H. M., Robert, N., Han, M., Puz̄rjova, I., Kollist, H., Lee, S., Mori, I., and Schroeder, J. I. 2013. Identification of cyclic GMP-activated nonselective Ca²⁺-permeable cation channels and associated CNGC5 and CNGC6 genes in Arabidopsis guard cells. *Plant Physiol.* 163:578-590.
- Wong, S. M., Chng, C. G., Lee, Y. H., Tan, K., and Zettler, F. W. 1994. Incidence of *Cymbidium mosaic* and *Odontoglossum ringspot viruses* and their significance in orchid cultivation in Singapore. *Crop Prot.* 13: 235-239.
- Yamaguchi, T., Minami, E., Ueki, J., and Shibuya, N. 2005. Elicitor-induced activation of phospholipases plays an important role for the induction of defense responses in suspension-cultured rice cells. *Plant Cell Physiol.* 46:579-587.
- Yu, H. H., and Wong, S. M. 1998. A DNA clone encoding the full-length infectious genome of odontoglossum ringspot tobamovirus and mutagenesis of its coat protein gene. *Arch. Virol.* 143:163-171.
- Zhang, C., Liu, Y., Sun, X., Qian, W., Zhang, D., and Qiu, B. 2008. Characterization of a specific interaction between IP-L, a tobacco protein localized in the thylakoid membranes, and *Tomato mosaic virus* coat protein. *Biochem. Biophys. Res. Commun.* 374:253-257.
- Zhang, Q., Lee, J., Pandurangan, S., Clarke, M., Pajak, A., and Marsolais, F. 2013. Characterization of Arabidopsis serine:glyoxylate aminotransferase, AGT1, as an asparagine aminotransferase. *Phytochemistry* 85: 30-35.
- Zhao, D., Ni, W., Feng, B., Han, T., Petrusek, M. G., and Ma, H. 2003. Members of the *Arabidopsis-SKP1-like* gene family exhibit a variety of expression patterns and may play diverse roles in Arabidopsis. *Plant Physiol.* 133:203-217.
- Zhou, H., Zhao, J., Yang, Y., Chen, C., Liu, Y., Jin, X., Chen, L., Li, X., Deng, X. W., Schumaker, K. S., and Guo, Y. 2012. Ubiquitin-specific protease 16 modulates salt tolerance in *Arabidopsis* by regulating Na⁺/H⁺ antiport activity and serine hydroxymethyltransferase stability. *Plant Cell* 24:5106-5122.
- Zybailov, B., Rutschow, H., Friso, G., Rudella, A., Emanuelsson, O., Sun, Q., and van Wijk, K. J. 2008. Sorting signals, N-terminal modifications and abundance of the chloroplast proteome. *PLoS ONE* 3:e1994.

AUTHOR-RECOMMENDED INTERNET RESOURCES

The Protein Structure Prediction server: ps2.life.nctu.edu.tw
 PyMOL molecular visualization system: www.pymol.org
 National Taiwan University's ContigViews web server:
www.contigviews.bioagri.ntu.edu.tw